NASA/TM—2002-211894

Methodology of Blade Unsteady Pressure Measurement in the NASA Transonic Flutter Cascade

J. Lepicovsky
QSS Group, Inc., Cleveland, Ohio

E.R. McFarland
Glenn Research Center, Cleveland, Ohio

V.R. Capece
University of Kentucky, Paducah, Kentucky

T.A. Jett
Glenn Research Center, Cleveland, Ohio

R.G. Senyitko
QSS Group, Inc., Cleveland, Ohio

October 2002

The NASA STI Program Office . . . in Profile

Since its founding, NASA has been dedicated to the advancement of aeronautics and space science. The NASA Scientific and Technical Information (STI) Program Office plays a key part in helping NASA maintain this important role.

The NASA STI Program Office is operated by Langley Research Center, the Lead Center for NASA's scientific and technical information. The NASA STI Program Office provides access to the NASA STI Database, the largest collection of aeronautical and space science STI in the world. The Program Office is also NASA's institutional mechanism for disseminating the results of its research and development activities. These results are published by NASA in the NASA STI Report Series, which includes the following report types:

- TECHNICAL PUBLICATION. Reports of completed research or a major significant phase of research that present the results of NASA programs and include extensive data or theoretical analysis. Includes compilations of significant scientific and technical data and information deemed to be of continuing reference value. NASA's counterpart of peer-reviewed formal professional papers but has less stringent limitations on manuscript length and extent of graphic presentations.

- TECHNICAL MEMORANDUM. Scientific and technical findings that are preliminary or of specialized interest, e.g., quick release reports, working papers, and bibliographies that contain minimal annotation. Does not contain extensive analysis.

- CONTRACTOR REPORT. Scientific and technical findings by NASA-sponsored contractors and grantees.

- CONFERENCE PUBLICATION. Collected papers from scientific and technical conferences, symposia, seminars, or other meetings sponsored or cosponsored by NASA.

- SPECIAL PUBLICATION. Scientific, technical, or historical information from NASA programs, projects, and missions, often concerned with subjects having substantial public interest.

- TECHNICAL TRANSLATION. English-language translations of foreign scientific and technical material pertinent to NASA's mission.

Specialized services that complement the STI Program Office's diverse offerings include creating custom thesauri, building customized databases, organizing and publishing research results . . . even providing videos.

For more information about the NASA STI Program Office, see the following:

- Access the NASA STI Program Home Page at ***http://www.sti.nasa.gov***

- E-mail your question via the Internet to help@sti.nasa.gov

- Fax your question to the NASA Access Help Desk at 301–621–0134

- Telephone the NASA Access Help Desk at 301–621–0390

- Write to:
  NASA Access Help Desk
  NASA Center for AeroSpace Information
  7121 Standard Drive
  Hanover, MD 21076

NASA/TM—2002-211894

Methodology of Blade Unsteady Pressure Measurement in the NASA Transonic Flutter Cascade

J. Lepicovsky
QSS Group, Inc., Cleveland, Ohio

E.R. McFarland
Glenn Research Center, Cleveland, Ohio

V.R. Capece
University of Kentucky, Paducah, Kentucky

T.A. Jett
Glenn Research Center, Cleveland, Ohio

R.G. Senyitko
QSS Group, Inc., Cleveland, Ohio

National Aeronautics and
Space Administration

Glenn Research Center

October 2002

Acknowledgments

The work was sponsored by the NASA Glenn Research Center under the Smart Engine Components Project managed by Mr. R.D. Corrigan as a part of the R&T Base Propulsion and Power Program. The authors would like to thank Mrs. L. Shaw, Chief, Turbomachinery and Propulsion Systems Division, for her continuous support.

Trade names or manufacturers' names are used in this report for identification only. This usage does not constitute an official endorsement, either expressed or implied, by the National Aeronautics and Space Administration.

The Aerospace Propulsion and Power Program at NASA Glenn Research Center sponsored this work.

Available from

NASA Center for Aerospace Information
7121 Standard Drive
Hanover, MD 21076

National Technical Information Service
5285 Port Royal Road
Springfield, VA 22100

Available electronically at http://gltrs.grc.nasa.gov

METHODOLOGY OF BLADE UNSTEADY PRESSURE MEASUREMENT IN THE NASA TRANSONIC FLUTTER CASCADE

J. Lepicovsky
QSS Group, Inc.
Cleveland, Ohio 44135

E.R. McFarland
National Aeronautics and Space Administration
Glenn Research Center
Cleveland, Ohio 44135

V.R. Capece
University of Kentucky
Paducah, Kentucky 42002

T.A. Jett
National Aeronautics and Space Administration
Glenn Research Center
Cleveland, Ohio 44135

R.G. Senyitko
QSS Group, Inc.
Cleveland, Ohio 44135

Summary

In this report the methodology adopted to measure unsteady pressures on blade surfaces in the NASA Transonic Flutter Cascade under conditions of simulated blade flutter is described. The facility was designed for this purpose, and previous test programs to study flutter have been conducted in the facility. Data from these previous programs proved to have some irregularities. To improve the quality of data taken in the facility, the cascade configuration was modified to improve the flow quality. Recent measurements show that the flowfield uniformity and blade loading periodicity were noticeably improved. Also, the facility was equipped with a completely new unsteady data acquisition system solely based on digital recording technology. New data acquisition and data reduction procedures were developed in-house. The experimental data were reduced to pressure-time history segments for each blade and pressure port. The previous work done in this cascade, before its modification, reported that the oscillating cascade produced waves, which for some interblade phase angles reflected off the wind tunnel walls back into the cascade, interfered with the cascade unsteady aerodynamics, and contaminated the acquired data. To alleviate the problems with data contamination due to the back wall interference, a method of influence coefficients was selected for the future unsteady work in this cascade. In this approach only one blade in the cascade is oscillated at a time.

The majority of the report is concerned with the experimental technique used and the experimental data generated in the facility. The report presents a list of all test conditions for the small amplitude of blade oscillations, and shows examples of some of the results achieved. The report is not a complete archival collection of unsteady pressure data acquired during this phase of experiments. All the acquired unsteady pressure data will be available in a suitable media form later. Also in the report is a description of the method of influence coefficients used to analyze unsteady flows, and a short discussion of a simple quasi-unsteady CFD simulation of the experiment that proved useful in planning the test program. The report does not discuss data analysis procedures like ensemble averaging, frequency analysis, and unsteady blade loading diagrams reconstructed using the influence coefficient method. Finally, the report presents the lessons learned from this phase of the experimental effort, and suggests the improvements and directions of the experimental work for tests to be carried out for large oscillation amplitudes.

Symbols

C	[mm]	blade chord
c_P	[1]	pressure coefficient
C_p	[1]	influence coefficient
g	[$m.s^{-2}$]	gravitational acceleration
h	[mm]	blade height
i_{FL}	[dg]	flow incidence
i_{GM}	[dg]	geometry incidence
k	[$mV.kPa^{-1}$]	slope of a calibration line
Ma	[1]	flow Mach number
p	[kPa]	unsteady pressure
p_W	[kPa]	wall static pressure
p_{1t}	[kPa]	cascade inlet total pressure
p_P	[kPa]	pressure side pressure
p_S	[kPa]	suction side pressure
q	[mV]	y intercept of a calibration line
s	[mm]	blade pitch
V	[$m.s^{-1}$]	flow velocity
W	[mm]	cascade test section width
x	[mm]	axial distance (cascade)
y	[mm]	pitchwise distance (cascade)
α	[dg, rd]	amplitude of blade oscillations
γ	[dg]	stagger angle
π_{TB}	[1]	cascade pressure ratio
ρ	[$kg.m^{-3}$]	density
θ	[dg]	leading edge camber angle
σ	[dg]	interblade phase angle

Abbreviations

AC	alternating current
ACM	accelerometer
A/D	analog/digital
DC	direct current
EDM	electro discharge machining
OPP	once per period
NI	National Instruments
PC	personal computer
UDSA	unsteady data acquisition system

1. Motivation

Modern turbofan engines employ a highly-loaded, low-aspect ratio fan stage with transonic or low-supersonic relative velocities in the blade-tip region. The tip-section airfoils of these fan blades are noticeably different from the airfoil sections on the rest of the blade. The tip-section airfoils are designed for precompression, with a concave suction surface just downstream of the leading edge, and with very low overall camber. The airfoils have a sharp leading edge that makes them prone to flow separation at off-design conditions. Due to extreme flight envelope requirements, the engines are often operated near the stall flutter boundary of the fan. At these conditions the fan tip section is subjected to high incidence angles and high subsonic or transonic relative Mach numbers. Blade flutter and associated high cycle fatigue problems result. These are very detrimental to the engine health and must be avoided. Stall flutter and particularly blade life prediction codes are not yet fully reliable; their verification is hampered by a lack of reliable unsteady loading data, particularly for the airfoils in question. Interest in fan blade stall flutter research has increased in recent years.

The NASA Transonic Flutter Cascade has been used to investigate behavior of a cascade of modern, low-aspect ratio fan blades operating near the stall flutter boundary that occurs at high incidence angles and high subsonic and transonic relative Mach numbers. A view of the cascade test section is in Fig. 1.1. The blades for this experiment were designed and manufactured by Pratt & Whitney Engine Company. The airfoil and cascade parameters are given in Fig. 1.2 and Tab. 1.1 (Ref. 1.1). Previous measurements on these blades were reported by Buffum et al. (Refs. 1.1 and 1.2) at Mach numbers between *0.5* and *0.8*, and chordal, geometric incidence angles, i_{GM}, of *0 dg* and *10 dg*. Experimental blade-surface pressure distributions for steady flow at inlet Mach numbers of up to *0*.5 were compared with various CFD predictions, but good agreement was found only up to 85% of chord and only for the incidence angle of *0 dg*. The cascade flow periodicity was measured only for the three middle blades and was found sufficient for unsteady surface-pressure data sets acquired at full-chord reduced frequencies of *0.4* and *0.8*, and for an interblade phase angle of *180 dg*.

The unsteady data, reported by Buffum et al. (Refs. 1.1 and 1.2), were acquired for oscillations of all nine blades. In older work done in this cascade Buffum and Fleeter reported (Ref. 1.3) that the oscillating cascade produced waves which for some interblade phase angles reflected off the wind tunnel walls back into the cascade and interfered with the cascade unsteady aerodynamics. Later, the tunnel was provided with perforated walls at several locations and acoustic treatment. The efficiency of this arrangement still has not been proven. Ott at al. (Ref. 1.4) recommended for their facility just the opposite: replacement of slotted walls with solid ones.

To alleviate the problems with data contamination due to the back wall interference, it was decided to adopt a method of influence coefficients for the future unsteady work in Transonic Flutter Cascade. The technique of influence coefficient technique is described in detail in Chapter 5. In this approach, only one blade in the cascade is oscillated at a time and the resulting unsteady pressures are measured on the remaining (nonmoving) blades. The unsteady aerodynamics of an equivalent cascade with all blades oscillating at a specified interblade phase angle is then determined through a vector summation of unsteady data from individual blades (Ref. 1.5). It must be stated that the use of the influence coefficient technique has only been demonstrated for attached flow. This facility has the unique capability of demonstrating this technique for separated flow. This technique requires a high degree of flow periodicity within the cascade for a larger number of blades.

2. Cascade facility upgrade

The NASA GRC Transonic Flutter Cascade is one of a very few test facilities dedicated to the unsteady aerodynamics of oscillating airfoils. The facility is used to provide data for modeling aerodynamics of blade stall flutter. The facility combines a linear cascade wind tunnel with a high-speed drive system that imparts pitching oscillations to cascade blades. The cascade consists of nine blades. All the blades or any single blade can be oscillated at realistic reduced frequencies (Strouhal numbers).

Interblade phase angles can be varied in increments of *15 dg*. The facility has been described in detail in works of Boldman and Buggele (Ref. 2.1), Shaw et al. (Ref. 2.2), and Buffum et al. (Ref. 1.1).

Improved cascade configuration

Recently, a systematic experimental and computational study (Refs. 2.3 through 2.5) was carried out with a goal of improving the quality of experimental data acquired in the NASA Transonic Flutter Cascade facility. In the study, available means for control and modifications of the cascade flowfield were fully investigated and analyzed. Further, several discrepancies in the older data sets were explained, particularly the questions of actual flow incidence angles and the inconsistency between predicted and measured backpressure levels. Several conclusions important for future work on unsteady pressure distributions in a cascade under stall flutter conditions were reached. The most important conclusions can be summarized as follows:

1. The boundary-layer bleed did not improve the flowfield uniformity and blade-load periodicity of the cascade tested. On the contrary, high bleed affected pitchwise distribution of flow incidence angles along the cascade and thus contributed to blade load variations.
2. The boundary layer bleed improves flow uniformity in the spanwise direction only in the vicinity of both sidewalls. The midspan section of the blade is not affected at all. For future experiments, it is recommended that the boundary-layer bleed system not be used.
3. The tailboard setting significantly affects the pitchwise distribution of static wall pressures and their levels.
4. The overall turning of the flow by the tunnel walls must match the cascade blades ability to turn the flow when operating as an infinite cascade. A mismatch between the wall turning and the blade's turning of the flow will result in walls interfering with the blade-to-blade periodicity of the cascade.
5. It is extremely important to match the tunnel wall contours with expected streamlines. This is particularly important for conditions of blade separated flows where it may not be readily obvious. Any mismatch between the cascade streamlines and tunnel contour walls results in a tunnel driven flow with the cascade under investigation having very little effect on the flowfield.
6. Flow incidence angles should be measured for each new configuration of the cascade facility. It is very risky to rely on geometric angles in determining the actual flow incidence.
7. By carefully tailoring tunnel wall contours to the expected streamlines for the current flow incidence of *10 dg*, the flowfield uniformity upstream and downstream of the cascade improved significantly. Further, very high blade load uniformity now extends over six blades from blade BL2 to blade BL7.

A schematic picture of the modified cascade configuration is in Fig. 2.1. Wall static pressures distributions for this configuration were very uniform as shown in Fig. 2.2 for three inlet Mach numbers of *0.5*, *0.8*, and *1.0*. The saw tooth character of the upstream pressure distribution for $Ma = 1.0$ indicates presence of shock waves emanating from the blade leading edges. The uniformity of wall static pressures in the pitchwise direction was a good indicator of an improved cascade flow periodicity for this configuration.

Instrumented blades

Six blades were instrumented for this study. Two blades were instrumented with conventional static taps, 15 ports along the midspan line, one blade on the suction surface (blade S1) and the other on the pressure surface (blade P1). Figs. 2.3 and 2.4 show location of static ports on blades S1 and P1. Four blades were instrumented with miniature high-frequency pressure transducers Kulite XCQ-062-15A with a nominal range of *0* to *100 kPa* absolute. The blades instrumented with Kulite transducer were labeled KS1 and KS2 for instrumented suction surface, and KP1 and KP2 for instrumented pressure surface of the blade. The batch of transducers for blades KS1 and KP1 had an average sensitivity of *1.3 mV/kPa* and the batch for blades KS2 and KP2 had an average sensitivity of *0.6 mV/kPa*. Locations of Kulite transducers were identical to blades S1 and P1 respectively. The blades were grooved before the Kulite transducers were flush mounted in the blades. The machining was done by the EDM (Electric Discharge

Machining) method. The EDM electrode and the grooved blade are shown in Fig. 2.5. Fig. 2.6 shows the KS2 and KP2 blades prior inserting the Kulite transducers. Finally, Fig. 2.7 shows fully instrumented blades KS2 and KP1.

As seen in Fig 2.7, the wires from Kulite transducers were routed through the mounting shaft of the blade. This is a challenge because once the instrumented blade is inserted into the cascade, altogether 60 wires per blade (4 wires per each transducers) must be routed from the blade shaft pass the driving cams out of the cam gear box that is filled with oil. Fig. 2.8 shows the open cam box on the back side of the cascade test section and the details of transducer leads (see Ref. 2.1 for details about the blade drive system). The lead wires were terminated with miniature 32 pin connectors (two per each blade) that enabled connections with the data acquisition system. The Kulite leads are only *0.1 mm* in diameter and quite fragile. To prevent wire damage during blade installations and operation of the cascade, the wires were cemented into the blade grooves and also in the shaft. Unfortunately, it turned the weakest point was at the back face of the blade shaft, where the wires exited from the cement filler. Many transducers were lost due to wire breaking at the shaft backface.

3. Data acquisition procedure

Two sets of data were acquired during the experiments: steady state data and unsteady data. The steady state data were acquired using the labwide ESCORT system (Ref. 3.1). The ESCORT data system monitors and records steady state cascade research data as well as of the facility operation data. The unsteady data were acquired using a test cell dedicated system that was tailored to the needs of this particular test setup. A requirement was to record the unsteady data in a digital form with a direct access to PC environment.

Unsteady data acquisition system

An overall diagram of the unsteady data acquisition system (UDAS) is shown in Fig. 3.1. The system was built around the National Instruments (NI) PXI Modular Instrumentation System. The PXI-1010 system was selected because it offers rugged, shielded construction that provides a low-noise environment for data acquisition and signal conditioning. The core of the system is an embedded data acquisition computer PXI-8156B with a *333 MHz* Intel Pentium processor and a *4 GB* hard drive. Two NI 6071E A/D (analog/digital) boards are controlled by the data acquisition computer. Each board accepts 64 single-ended analog inputs, which means that up to 32 Kulite transducer can be connected to a board because each Kulite transducer requires a differential input (two channels per a transducer). The board has 12-bit resolution, it is 4096 discrete voltage levels. The scanning frequency is quite high *1.25 MHz*, which allows sampling frequency for any of the 32 differential channels to go up to *39 kHz*. The boards communicate with the data acquisition computer PXI-8156B via an internal bus at *1.25 MS/s*.

Each Kulite transducer had an allocated amplifier for signal conditioning. Endevco 4430A programmable bridge transducer signal conditioners were selected. This conditioner is a precision DC bridge amplifier with built-in constant excitation voltage/current supply and a programmable low pass filter. All the Kulite signal amplifiers were set for DC amplification of *50* for blades KS1 and KP1, and *100* for blades KS2 and KP2. Low pass filters and zero offsets were disabled. An oscilloscope Tektronix 2465B was used to monitor live signals.

The UDSA system was controlled by in-house developed software. All data acquisition and reduction software procedures were written in programming language G (NI Labview). Data acquisition time for each test point was *3150 ms*, which is 120,000 samples. Raw data for each blade were stored in binary files in a spreadsheet form with 16 columns (lead signal plus 15 pressure transducers). The file size is *7.5 MB*. In order to maintain the high speed of data sampling of *38 kHz*, the A/D boards were operated one at a time. It means that for each cascade operating condition to sets of data were acquired.

First one recorded board #1 data (blades KS1 and KS2), and the second one recorded data for board #2 (blades KP1 and KP2).

Data acquisition timing

The timing of data acquisition is depicted in Fig. 3.2. It is identical for both A/D boards. In this diagram, the elapsed time is shown on the horizontal axis, and the sequence of 32 channels per board on the vertical axis. Starting in the lower left corner, the first signal to acquire is the once per period (OPP) signal, which is once per blade oscillation period mark. The OPP signal is the lead signal for blade #1. The second signal to be recorded is the transducer #1 on blade #1 (KS1 for board #1 or KP1 for board #2). The time difference between these two signals is *0.8* which corresponds to the *1.25 MHz* scanning frequency. The signals from the rest of the transducers on the blade are recorded in the same sequence. As seen in the picture, it takes *11.2 μs* to record data from all the transducers on one blade. Channel 17 on this board records ACM signal, which is the accelerometer signal located on the tip shaft of the blade BL5, it is the blade that is oscillated. The purpose of this signal is to verify the position of the oscillating blade with respect to the recorded pressure time histories on the instrumented blades. The ACM signal is the lead signal for blade #2. Signals from pressure transducers on blade #2 are recorded in the same sequence as on blade #1. It takes all together *24.8 μs* to record pressure data from both blades including OPP and ACM signals. The remaining *1.5 μs* the system idles to complete the time period of *26.3 μs*, which corresponds to the sampling frequency of *38 kHz*. This cycle is repeated 120,000 times to complete one test point. There were two accelerometers available for some of the runs. For those test points, the accelerometer ACM_1 was allocated to board #1 and accelerometer ACM_2 to board #2. For the OPP signal however, it was the same signal that was always allocated to both boards. This signal serves as a synchronizer for the time history signals from two separate boards. This allocation scheme was maintained during the entire test program. Even if a transducer was lost, the timing sequence stayed the same, and the faulty transducer data was removed only during the postprocessing procedures.

Blade ‘zero’ angle

Beginning of data acquisition is triggered randomly, and therefore the knowledge of the phase between the OPP mark and the blade angular position is important to establish zero for blade oscillations. Fig. 3.3 explains the phase relation between the oscillating blade and the OPP signal for the amplitude of blade oscillations of *0.6 dg*. In the upper left corner, the blade is at *30.0 dg* with respect to the horizontal plane. This is the blade ‘zero’ angle. During one period of blade oscillation, the blade angle first increases to *30.6 dg*, then decreases to *29.4 dg*, and returns back to *30.0 dg*. The blade oscillation is forced by rotation of a camshaft (Fig. 2.8). The gear ratio is 6:1, it means that for one cam shaft revolution the blade oscillates six times. The cam shaft is provided with a hexagon contour section at the very end. A proximity capacity sensor faces the hexagon surface and generates OPP signal. Time history of the OPP signal for blade oscillating frequency of *200 Hz* is shown at the bottom of Fig. 3.3. In this diagram, the interval between two adjacent peaks corresponds to one blade oscillation period, interval between every sixth peak corresponds to one camshaft revolution. The angular position of the proximity sensor was arbitrary with respect to the hexagon surface but stayed the same for the entire test program. Rotating the camshaft to the nearest hexagon vertex (to the nearest peak in time history plot) causes blade to move to an angle of *30 dg 31 min*. From the above data one can determine the blade ‘zero’ angle instant in the OPP signal time history. For example, for *200 Hz* oscillating frequency, the blade passed through the ‘zero’ angle *1.08 ms* past any peak instant in the OPP time history. Because the time history of the OPP signal is firmly connected with the time history of any signal on the same A/D board by the board hardware clock (Fig. 3.2), the ‘zero’ blade position can be uniquely determined for any pressure history data. The direction of cam rotation during the pressure data acquisition is indicated in Fig 3.3 by a contoured arrow.

Transducer calibration

A general impression is that the miniature pressure transducers, like Kulites, are suitable mainly for measurement of pressure fluctuations and the steady state pressure levels are not very reliable. Usually, AC amplifiers amplify signals from Kulite transducers, and the information about the 'DC' pressure level is then lost. This approach evolved in the past due to a low resolution of the A/D boards used in data acquisition systems. The range and resolution of the NI A/D board 6071E used in the UDSA system, however, is large enough to record the absolute output voltage using DC amplifiers. The resulting pressure resolution is better than *24 Pa*, which is fully sufficient. For comparison, the labwide steady state data recording system ESCORT has a resolution of *20 Pa* for *100 kPa* transducers. By recording absolute voltage output one can retrieve the information about steady-state pressure values as well as about the pressure fluctuations. By comparing the average absolute pressure levels with levels recorded by conventional static taps, it is possible to assess reliably the accuracy of measured pressure fluctuations.

Extensive calibration tests of transducers embedded in the instrumented blades were carried out in a vacuum chamber. The tests were time consuming because the blades had to be dismounted from the cascade for each calibration test. Only one blade could be tested at a time. As an example of calibration results, Fig. 3.4 presents data blade KP1, ports 6 and 10. The figure shows the calibration curves and deviation scatter. The results of four calibration tests of blade KP1 are summarized in Tab. 3.1. As seen here, the calibration constants drift a little. The slope of the calibration curves is relatively stable; the scatter is about 0.2% of the fullscale (FS) value, which is *200 Pa*. The scatter of zero offsets (y_0, y intercept) shows a larger value, up to 0.6% of FS (*600 Pa*). To improve the accuracy of voltage/pressure conversion for Kulite transducers the transducers should be calibrated just prior each test run. This was impractical so for the slope value the results of the last calibration tests were used. For the zero drift, however, new 'zeros' were read prior each test and used for the pressure conversion. In this way, the accuracy of the steady state pressures (time average pressures of Kulite readings) improved noticeably. As an illustration, Fig. 3.5 shows a comparison of five tests of three blades. The plots are in a form of pressure coefficient (c_p) distributions over a suction surface of the cascade blade BL4 for the inlet Mach numbers *0.5* and *0.8*. The data collapse between the conventional tap data and four Kulite data is very good; the largest difference appears to be for port 6. In terms of the pressure accuracy the maximum difference between the static tap and averaged Kulite data for port 6 is less than 2% of the local dynamic pressure value for Mach number *0.5*, and about 5% of the local dynamic pressure value for Mach number *0.8*. In terms of absolute local pressure values the tap/Kulite agreement is 0.4% for Mach number *0.5*, and 3.4% for Mach number *0.8*. The good agreement of Kulite averaged pressure values with the static tap values is a measure of accuracy for pressure fluctuations measured by Kulites. It is estimated that the accuracy of the pressure fluctuation amplitude measured by Kulite transducers (the AC component of the signal) is better than 2% of the local amplitude value.

4. Data reduction procedures

Signals from all pressure transducers were digitized and recorded as voltage levels. A low voltage unsteady signal is very sensitive to contamination due to electric ground loops and radio frequencies in general. All precautions were made to eliminate ground loops and properly shield all signal carrying wires, nevertheless some signals exhibited contamination and spurious spikes that could not be associated with flowfield pressure changes. Raw voltage signals were first converted to pressures, then in-house developed data cleaning procedures were applied to remove obvious signal contamination, and finally pressure levels were corrected for transducer zero drifts. All steps during the data reduction process were recorded in the data file header, and the original 'uncleaned' data are also available for comparisons.

Data reduction process consisted from four procedures. They were:
a. Voltage / pressure conversion,
b. Data clipping,
c. Data patching,
d. Mean pressure correction.

Voltage/pressure conversion

The voltage/pressure conversion procedure performs several functions. First, it retrieves voltage data for a selected port from a binary raw data blade file. Then, it converts voltage data to pressure units using the calibration constants as recorded in the latest calibration data file for a selected port. Next, it generates time variable based on the selected sampling frequency. Finally, it stores the pressure data as a function of time (pressure history) in a ASCII data file, that is labeled to indicate cascade configuration (blade position), blade label, port number, and test number that reflects operating conditions (data labeling convention is explained in Chapter 7). The output files are identified by an extension "hr3". The length of the entire record is *3000 ms*. Fig. 4.1 shows a *1000-ms* and a *100-ms* intervals of a raw uncontaminated signal.

Data clipping (signal local overshoots, single point spikes)

The signal clipping procedure is based on the following observation. Visualization of the cascade flowfield revealed noticeable flow instabilities for inlet Mach numbers in a range from *0.93* to *1.03*. For these inlet flow conditions, the shock wave pattern in the cascade is very unstable and exhibits rapid switching among individual blade channels (Ref. 4.1). This flow instability is strongest on the blade suction side close to the leading edge. Switching between the supersonic and subsonic flows in this region causes rapid changes in the local static pressure in the same region. The static pressure is at a low level for supersonic inlet flow and jumps to a high-pressure level when the flow drops to a subsonic velocity. Fig 4.2 shows the pressure jumps as recorded at port 1 for an average inlet flow at Mach number of *0.97*. As seen here, the rapid pressure changes are of the order of *20* to *25 kPa*. Even that these pressure jumps are the fastest pressure changes in the cascade, they do not happen instantly but over an interval of *300* to *350 μs*. As discussed above, the pressure signal was sampled at *38 kHz*, which means that two adjacent data points are *26.3 μs* apart. In other words, the fastest pressure changes are stretched at least over 12 sampling periods. Therefore, a pressure change between any two consecutive samples cannot be larger than *1.6 kPa,* maybe *2.0 kPa* at maximum. Data clipping procedure was built on this fact. The procedure marches through the recorded data and examines every sequence of three consecutive data points. If the middle point exhibits pressure overshoot above or below a selected value, the data point is removed and replaced by an average of it's pre- and post-neighbors. It should be stressed here, that the clipping procedure does not affect the timing of the data sequence and corrects only a single point over or under shoots. An example is shown in Fig. 4.3a,b. The data files that were modified by clipping have an extension "hc3".

Data patching (temporarily signal dropouts)

"Single point" over- or undershoots, however, were not the only data contamination observed. Some of the transducers exhibited occasionally behavior resembling a temporarily open circuit overcompensated by an amplifier feedback resulting in saturation of the A/D board input. An example of such behavior is in Fig. 4.4. These signal 'drop-outs" sometimes lasted over several sampling periods. Reasons for this behavior are still unclear, perhaps momentary disruptions of continuity either on the transducer bridge or in lead wires and connectors. Because the signal was contaminated over several sampling periods, the clipping procedure does not clean the signal, as demonstrated in Fig. 4.5. The signal outside of the saturation instants appeared healthy, and therefore a procedure was established to recover the undisturbed portion of the signal. The patching procedure is based on an assumption that a signal that represents true pressure cannot exceed minimum and maximum thresholds that defined a band about a mean pressure level. Fig. 4.6 illustrates this assumption. If the signal exceeds the selected thresholds, then the portion of the signal above the upper threshold (or below the lower threshold) is removed and the missing portion is replaced with a straight line connecting the endpoints of the patch, as shown in Fig. 4.7. This procedure, similarly as data clipping, does not alter the timing of the data sequence. This procedure, however, will slightly affect the variance of the signal. The saturation drop-outs extend only over few percent of the data collection interval. It is believed that the effects on the variance

of the undisturbed signal are insignificant. The data files that were subjected to patch procedure have extension “hp3”.

Zero drift correction

The last procedure corrects the pressure values for transducer zero drift that may be different from the calibration data. Before each test, zeros for all Kulite transducers were recorded. These readings, instantaneous zero offsets, respectively their differences from the zero offset recorded during the last previous Kulite calibration, were applied to the pressure values stored in the last modified data file (either “hc3” or “hp3” files). This procedure affects only the pressure average value (DC component of the signal). Magnitude of pressure fluctuations (the AC component) is not affected at all. The output file from the mean pressure correction procedure was labeled “hx3”. These are the files that should be used for additional data analysis including ensemble averaging, frequency analysis, unsteady blade loading, influence coefficient method, etc.

5. Influence coefficient method

In the previous cascade experiments by Buffum, Capece, King, and EL-Aini (Refs. 1.1 and 1.2) only an interblade phase angle of *180 dg* was reported. Experimental results at other interblade phase angles were judged to be unrealistic due to tunnel sidewall reflections. To expand the range of interblade phase angles possible, the influence coefficient method will be explored.

The influence coefficient method is based on the superposition principle for linear systems. For this case the unsteady pressures on an airfoil for a given cascade geometry, reduced frequency, and inlet flow condition are separated into a contribution of the airfoil oscillating on itself and a separate contribution from the oscillation of each neighboring airfoil. Hence, the unsteady aerodynamic perturbations generated in a cascade with all airfoils oscillating can be represented as the sum of perturbations generated by oscillating the airfoils individually. The situation where all airfoils are oscillating at a constant interblade phase angle is typically referred to as the traveling wave method.

The influence coefficient method has been used numerically and experimentally. For example, in a three dimensional numerical example for a compressor blade in supersonic inviscid flow, Gerolymos (Ref. 5.1) has shown that the influence coefficient method using 7 blade passages gives nearly equivalent first harmonic pressure coefficient results as the traveling wave method.

Many investigators have conducted experimental studies directed at validating the influence coefficient method. Some detailed studies have been conducted by Buffum and Fleeter (Ref. 5.2), Bolcs, Fransson, and Schafli (Ref. 5.3) and Fransson (ref. 5.4). Buffum and Fleeter (Ref. 5.2) used biconvex airfoils. Bolcs et al. (Ref. 5.3) and Fransson (Ref. 5.4) used an annular cascade with a variety of different turbine configurations. In general, the results have indicated the validity of the influence coefficient method for attached flow for cases where the wind tunnel sidewalls for linear cascade have a negligible influence and for unsteady flows that are not in the vicinity of acoustic resonance.

Theory

The influence coefficient method can be used for any of the oscillating airfoil response coefficients, e.g. unsteady aerodynamic lift, unsteady aerodynamic moment, or unsteady surface pressure. For the present investigation the first harmonic unsteady surface pressure coefficient is of fundamental interest.

Mathematically, the relation between the unsteady surface pressure coefficient influence coefficient and the unsteady surface pressure coefficient for all airfoils oscillating at a constant interblade phase angle (σ) is given by Eq. 1.

$$C_p(x,\sigma) = \sum_{n=-N}^{N} C_p{}^n(x) e^{in\sigma} \tag{1}$$

Where

$C_p(x,\sigma)$ is the complex value unsteady surface pressure coefficient at a given chord location (x) acting on the reference airfoil with all airfoils oscillating at a constant interblade phase angle (σ);

$C_p{}^n(x)$ is the complex valued unsteady surface pressure influence coefficient at the same chord location, which is the influence that oscillations of airfoil n have on the unsteady surface pressure coefficient of the reference airfoil;

N is the number of airfoils summed.

For an infinite cascade N is infinity. In the present case of the NASA Transonic Flutter Cascade, which has nine airfoils, N will be a maximum of four. Note that this relation has the form of a Fourier transform.

The influence coefficients can be determined from mathematical models for an infinite cascade of airfoils oscillating with a constant interblade phase angle. For this case the mathematical relationship is determined by inverting the Eq. 1.

$$C_p{}^n(x) = \frac{1}{2\pi}\int_{-\pi}^{\pi} C_p(x,\sigma) e^{-in\sigma} d\sigma \tag{2}$$

This relation can be used to determine analytical influence coefficients. Substitution of the analytical influence coefficients into Eq. 1 yields analytical results for a finite number of airfoils oscillating in an infinite cascade.

Experimental procedure

The experimental procedure to determine the unsteady surface pressure influence coefficients will now be discussed. The numbering system is illustrated in Fig. 5.1 for an infinite cascade where the "center" airfoil has been selected as the reference airfoil, *n = 0*. The influence coefficients are determined in a sequential manner. To determine the influence of the reference airfoil oscillating on itself $C_p{}^{n=0}(x)$, the reference airfoil is oscillated with all other airfoils held stationary, as depicted schematically in Fig. 5.2. In an analogous manner, the influence of oscillating airfoil *n = +1* with all other airfoils held stationary on the reference airfoil is determined, $C_p{}^{n=1}(x)$. This procedure is repeated for as many other influence coefficients as desired. The unsteady surface pressure influence coefficients are then substituted into Eq. 1 to determine the unsteady surface pressure coefficients at a constant interblade phase angle in the traveling wave mode.

To validate the influence coefficient method experimentally the cascade will be operated at interblade phase angles where the effect of acoustic wall reflections on the measured unsteady pressures

is negligible. This will be quantified by verifying the dynamic periodicity of the airfoils in the central portion of the cascade. The influence coefficient technique will be used with Eq. 1 and the results correlated with the experiments performed with all airfoils oscillating at a constant interblade phase angle. An oscillation amplitude of *0.6 dg* will be used. For this small of an oscillation amplitude the unsteady flow is assumed to be linear. This assumption will be evaluated in this investigation. To quantify the influence of oscillation amplitude these experiments will be repeated for an oscillation amplitude of *1.2 dg*, and selected experiments will be done at an oscillation amplitude of *2.4 dg*.

By using the influence coefficient technique interblade phase angles will be achievable that were not previously possible. This will allow the attainment of experimental data to further our understanding of the flow physics for unsteady separated flow.

To complete this section an alternate method for obtaining the influence coefficients using two instrumented airfoils is illustrated schematically in Fig. 5.3. This arrangement will yield the $n = +1$ and $n = +2$ influence coefficients. It can be seen that other influence coefficients can be easily obtained by moving the instrumented airfoils to other positions in the cascade. An attractive feature of this procedure is that it keeps the oscillating airfoil in the center of a finite cascade, which will minimize any acoustic wave reflections from the cascade sidewalls. In an infinite cascade this method is satisfactory and all the influence coefficients can be obtained by oscillating a single airfoil. However, for a finite number of airfoils there will be concerns with airfoils that are in the vicinity of the walls. In this region the airfoils will not be behaving as if they are in a cascade. Hence, the oscillating airfoil and instrumented airfoils will be shifted within the cascade to assess this difficulty.

Analytical influence coefficients

To complete this chapter analytical influence coefficients will be determined. The analytical influence coefficients will indicate how fast the influence coefficients decay as the oscillating airfoil moves away from the reference airfoil.

The mathematical model used for the infinite cascade is the flat plate semi-analytical analysis given by Smith (Ref. 5.5). This model is for two dimensional inviscid compressible flow. For this example the present cascade configuration is used. Since the model is inviscid the flow will be attached, and the incidence angle is zero; i.e., no steady aerodynamic loading. A Mach number of *0.5* is used with a reduced frequency based on semi-chord of 1. The cascade stagger angle is *60 dg*.

The magnitude of the unsteady surface pressure difference influence coefficients determined using Eq. 2 are presented in Fig. 5.4. The influence coefficients are determined for N = 5. Note that the largest influence coefficient is for $n = 0$, the influence of the reference airfoil oscillating on itself, $\Delta C_p^{n=0}(x/c)$. The next largest influence coefficient is for $n = -1$, with a rapid decay in the influence coefficients as the airfoil that oscillates moves further from the reference airfoil. For this example, the influence coefficients are mostly negligible for $|n| > 2$.

These influence coefficients are now summed using Eq. 1 and compared to the constant interblade phase angle calculation for interblade phase angles of *0 dg* and *180 dg*. For an interblade phase angle of *0 dg* acoustic wave are propagating away from the cascade into the far field. The summation in Eq. 1 was taken to be for $N = 2$, and $N = 5$, and the results are presented in Figs. 5.5 and 5.6. These results indicate that in both cases the influence coefficient series is rapidly convergent and that the reference airfoil and its immediate two neighbors have the most significant effect on the unsteady pressure difference coefficient. Furthermore, the influence coefficient summation exhibits excellent correlation with the traveling wave method. Moreover, the summation with $N = 2$ was sufficient except near the leading edge (where there is a square root singularity in the pressure distribution) for $\sigma = 0$ *dg*.

6. Simplified CFD analysis

When improving the flow quality of the facility, a two dimensional computer simulation of the test section was developed. The integral equation method described by McFarland (Refs. 6.1 and 6.2) was used. The simulation included the nine cascade blades and the tunnel walls. Since the solution technique does not require a computational grid and is very fast running, it provided a means for quickly looking at the effects variations in the test section geometry had on the periodicity of the flow. Figs. 6.1a and 6.1b illustrate the simulation of the test section. When combined with more sophisticated Reynolds averaged Navier Stokes CFD methods of Chima (Refs. 6.3 and 6.4), the CFD simulation proved very useful in achieving the goal of improving the flow quality and in understanding the test section flow.

Early in the unsteady test program, confidence in the unsteady instrumentation had not been established and the response of the flow field to the blade oscillation was unknown. When no response was initially being measured on the leading edges of the blades located three blades away from the central oscillating blade, concerns were raised that the instrumentation was faulty or that the experimental technique of oscillating a single blade was not good.

In order to resolve these concerns, a simple modification of the integral equation method was developed that produced a quasi-unsteady simulation of the oscillating flow. This was accomplished by adding the equation of motion of the oscillating blade. This allowed the position of the blade and its velocity relative to the stationary blades and tunnel walls to be calculated for any arbitrary point in the oscillation cycle. This information was used to alter the previous stationary blade simulation by modifying the surface velocity boundary conditions according the blades position during an oscillation. The result was an instantaneous look at the potential effect the blade oscillation had on the flow field.

The results of the calculations gave the location and the magnitude of variations in the flow field caused by the moving blade at a specific position in the oscillation cycle. A typical sequence of solutions is shown in Figs. 6.2a, b and c. The test condition for the figures is inlet Mach number of *0.8*, oscillating frequency of *500 Hz*, and maximum deflection of *0.6 dg*. The first figure shows the blade at maximum deflection, leading edge moved *0.6 dg*, to the right and at zero rotational velocity, as the blade is about to change direction. The middle figure shows the flow field with the blade at *0 dg* deflection, but at maximum rotational velocity. The last figure shows the blade at maximum deflection to the left. Timing or phasing information cannot be determined from the solutions since time is not a variable in the solution. Any potential effect appears to occur through out the flow field instantaneously in the calculation.

The entire test matrix for the two subsonic inlet Mach numbers of *0.5* and *0.8* were calculated. Four frequency (*200*, *300*, *400* and *500 Hz*) and three deflection angles (*0.6*, 1.2, and *2.4 dg*) were calculated for these Mach numbers. A summary of the results of these calculations are presented in Fig. 6.3.

Finally animations were made using the simulations. A series of solutions were made for the blade as it moved through one oscillation. Contour plots similar to those shown in Fig. 6.2 were made for each blade position in the series. When these are shown in rapid sequence the contour lines appear to be in motion. The locations in the simulation where the lines appear to be moving the most highlight the regions where unsteady flow variations will occur. These animations proved very useful in determine where to expect a high amount of signal response from the Kulite sensors, and also regions where the response from the sensors will be little. The animations also indicated test conditions where reflex of the unsteady pressure waves by the wall may occur.

7. Samples of experimental data

Test matrix

Two sets of unsteady pressure data were acquired during the first phase of this experimental work. In the first set no blade in the cascade was oscillated and the inlet Mach number was gradually raised from *0.4* to *1.1*. In the second set, the middle blade (blade BL5) was oscillated at frequencies *200*, *300*, *400*, and *500 Hz* for the inlet Mach numbers of *0.5*, *0.8*, *1.0*, and *1.1*. Blade BL5 was oscillated at a single amplitude of *0.6 dg*. A simplified test matrix is shown in Tabs. 7.1 and 7.2. All test conditions for nonoscillating blade data are listed. For the oscillating blade data, the actual test matrix consists of all possible combinations of test parameters listed in Tab. 7.2.

For both data sets, the blade BL5 was always the uninstrumented one. The Kulite instrumented blades KS1, KS2 (suction side), and KP1, KP2 (pressure side), as well as the blades instrumented with conventional static taps S1 (suction side), and P1 (pressure side) were randomly placed in blade positions BL2, BL3, BL4, BL6, BL7, and BL8 for recording pressure data throughout the cascade. Tab. 7.3 presents a list of blade positions for this phase of the experiment. The middle blade (BL5) is labeled FB (flutter blade). The last column designates the data group. This is the key to allocate the instrumented blade positions to individual test runs.

Data labeling convention

The following labeling convention was adopted for data assignment:

C*n_gg_tt*_K*bb_pp*.h*fi* (example C1_35_14_KS1_03.hx3)

Here, the first letter (C) denotes cascade data; the following number denotes cascade configuration (e.g. *n* = 1 means incidence *10 dg* and oscillation amplitude *0.6 dg*). Next, the data group is listed (e.g. *gg* = 35 designates test group run on 11-Apr-00 when the blade KS1 was in blade position BL 4 as can be found in Tab. 7.3). This is followed by a test run sequential number (e.g. *tt* = 14). The test sequential number has no special meaning except of distinguishing individual test runs. The following group (K*bb*) designates Kulite instrumented blade (e.g. K*bb* = KS1, means blade #1 instrumented with Kulite transducers on the suction surface). Each instrumented blade had 15 pressure ports as shown in Figs. 2.3 and 2.4. The pressure port is given next (e.g. *pp* = 03, means third pressure port counted from the blade leading edge). The file name extension has the following meaning: the first letter (h) denotes time-history data, the next letter (*f*) determines the type of data as far as data reduction and cleaning procedures are concerned (e.g. r = raw data, c = clipped data, p = patched data, and x = zero correction

data). Finally, the last digit (*i*) determines the time interval of the pressure unsteady data (e.g. 3 = *3000 ms* of continuous data). In general all data that will be released to the public domain for additional data reduction, including conditional sampling and frequency analysis, will have extension ***hx3***.

Unsteady pressure data for no blade oscillations

A serious of test data for blade KS1 and pressure port 01 for the case of no blade oscillation is shown in Fig. 7.1. The figure shows a series of data records for an increasing inlet Mach number ranging from *0.5* to *1.02*. Only the interval of *200 ms* is shown for clarity. The presented pressure data are for pressure port 01 on blade KS1 (KS1_01 data files). Static pressures for the same port acquired by a conventional surface tap (blade S1) showed a continuous and smooth pressure drop through the transonic region as the inlet Mach number was raised. Such data indicate that the local flow velocity, just downstream of the leading edge, continuously increases from subsonic to low supersonic values. This indicated continuous velocity increase, however, contradicts the observed unsteady and intermittent behavior of the flow shock pattern for transonic inlet flow conditions (Ref. 4.1). Furthermore, surface flow

visualization using a oil-paint mixture clearly shows that for the subsonic inlet Mach numbers there is a large separated flow region on the blade suction surface just past the leading edge exhibiting a complex three-dimensional flow structure (Ref. 4.1). For the supersonic inlet flow, however, the flow past the leading edge is fully attached to the blade on a considerable length. This abrupt change of surface flow patterns is also not indicative of a smooth velocity increase through the transonic flow region.

Unsteady pressure levels at port 01, presented in Fig. 7.1, show pressure behavior that is not indicative of a smooth velocity flowfield in the high subsonic and transonic flow regions, and perhaps give new insight in the physics of the subsonic to supersonic flow transition. For lower inlet Mach numbers ($Ma < 0.85$) the local flow past the blade leading edge is always subsonic with increasing velocity fluctuations in the separated flow region. Starting at this inlet flow Mach number, local pressure begins to drop temporarily below the level at which the flow reaches low supersonic velocities. These bursts of supersonic velocity are at first very short (a few milliseconds) and infrequent. With increasing inlet Mach number, however, the duration and number of appearances of supersonic flow velocities increases dramatically. For an inlet Mach number of about *0.95* to *0.97*, the local flow velocity at the blade leading edge is supersonic half of the time. However, it appears that the velocity is still switching randomly and is of variable duration. As the Mach number increases further the regions of supersonic flow velocity rapidly lengthen with very sporadic instances of subsonic velocity pockets.

The jumps in the local pressure level in the blade leading edge region are about *20* to *25 kPa* for the Mach number range from *0.9* to *1.0*. It appears that the flow in the high subsonic and transonic region is bistable, randomly switching between the subsonic and supersonic flows. The smooth pressure drop in this region measured by the conventional static taps is an artifact of the averaging process of this pressure measuring method. It appears that in reality the change in overall flow conditions in the transonic flow region is based on the frequency of switching between two stable flow states rather than on the continuous increase of the flow velocity.

To the authors' knowledge this phenomenon of pressure bistability in the leading region of a transonic cascade was not reported yet. Pressure jumping between two levels in the transonic region generates large intermittent loading on the blade leading edge region and can lead to the onset of blade torsional oscillations resulting in severe flutter. At the moment, it is not clear if this is a real phenomenon in an annular transonic fan cascade or a 'byproduct' of a span restricted linear transonic cascade. The acquired data will be thoroughly analyzed before a final judgment can be reached. In any case, this new model of the flow physics in the transonic fan blade cascade will either impact computational methods for flutter predictions in transonic fans or limit the use of linear transonic cascade data to regions outside of the range of pressure bistable behavior.

Unsteady pressure data for middle blade oscillations

In this group of experiments the middle blade (blade BL5) was oscillated at frequencies *200*, *300*, *400*, and *500 Hz* for the inlet Mach numbers of *0.5*, *0.8*, *1.0*, and *1.1*. Blade BL5 was oscillated at a single amplitude of *0.6 dg*. The following examples of unsteady pressure data are for blade KS1 located in position BL4, it is for $n = -1$ in terms of the influence coefficient method (see Chapter 5).

The effects of blade oscillation frequency (blade BL5) are shown in Fig. 7.2. The segments *100 ms* long of pressure data for port 15 (the closest port to the airfoil trailing edge) are shown here for the case of no oscillations and oscillations of *200*, *300*, and *400 Hz* for the inlet Mach number of *1.08*. It should be stressed that the shown data are pure time histories, not enhanced by ensemble averaging. Several observations can be made here. First, the pressure signal for case of no oscillations (C1_42_95_KS1_15) exhibits weak contamination due to modulation by the net frequency of *60 Hz*. Peak-to-peak variation of the signal contamination is about *2 kPa*. The distributions acquired for blade BL5 oscillating at *200*, *300*, and *400 Hz* show very strong modulation due to the oscillating blade frequency. The peak-to-peak variations of the modulated signal are *9 kPa* for frequencies of *200* and *300 Hz* (data files C1_42_96_KS1_15 and C1_42_97_KS1_15), and about *7 kPa* for the case of *400 Hz* (data file C1_42_98_KS1_15).

The situation for the subsonic inlet Mach number of *0.8* is depicted in Fig. 7.3. Here the signal for no blade oscillations (C1_42_32_KS1_15) exhibits very strong modulation at frequency of *91 Hz* and peak-to-peak variation of *11 kPa*. Pressure distribution acquired at port 01 on the same blade and the same inlet Mach number (data file C1_36_17_KS1_01 in Fig. 7.1a) does not exhibit any periodic modulation at all. It is very doubtful that the observed pressure fluctuations at pressure fluctuations experienced by the trailing region of the airfoil for this flow conditions. It should be stressed that this is a preliminary conclusion and the data will be subjected detail analysis before a final statement can be made. Introducing blade oscillations of *200 Hz* does not visibly change the character of the signal (C1_42_33_KS1_15). For higher frequencies of blade BL5 oscillations, the effects of blade oscillations are traceable (data files C1_42_35_KS1_15 and C1_42_36_KS1_15). In particular, for the highest blade frequency, a modulation of *500 Hz* is superimposed on the signal and is traceable. The peak-to-peak variation of *500-Hz* modulation is about *5 kPa*.

Finally, data for the lowest inlet Mach number of *0.5* are shown in Fig. 7.4. The case of no blade oscillations shows contamination by the net modulation of *60 Hz* (C1_42_13_KS1_15). The peak-to-peak variation is about *2 kPa*. The effects of forced oscillations are barely traceable for the blade frequency of *200 Hz* (C1_42_14_KS1_15), however, they are clearly visible for the cases of blade frequency of *400* and *500 Hz* (data files C1_42_16_KS1_15 and C1_42_17_KS1_15). However, the peak-to-peak variation of the forced signal modulation is quite small, about *2 kPa*.

Changes in the character of the unsteady pressure signal from port to port along the blade chord are shown in Fig. 7.5 for the case of a supersonic inlet Mach number of *1.08* and the forcing frequency of *400 Hz*. The first pressure distribution is for Port 01, which is very close to the blade leading edge (data file C1_42_98_KS1_01). The signal is very clean, uncontaminated and correctly shows no effects of the oscillating blade BL5; for the supersonic inlet condition any pressure fluctuations generated at the leading edge of blade BL5 cannot propagate to the leading edge region of blade BL4. Signals from ports 05 and 06, however, already show effects of forced pressure modulation (data files C1_42_98_KS1_06 and C1_42_98_KS1_07). The peak-to-peak modulations are about *3 kPa* and *4 kPa*, respectively. The signal for Port 15 (data file C1_42_98_KS1_15) was already discussed above, and shows the strongest modulation of *7 kPa* peak-to-peak.

It can be stated, based on this very short overview, that the presented pressure distributions for blade $n = -1$ appear to follow some of the predictions made using the simplified CFD analysis. The predicted results are summarized in Fig. 6.3. The discussed unsteady pressure distributions show that peak-to-peak variations of the forced modulation increase with an increasing inlet Mach number. For the blade suction side, the amplitude of forced modulation is larger for the pressure port at the blade leading edge than for the blade midchord region. Finally, there seems to be little effect of the forcing frequency level on the amplitude of forced modulation. Of course, these are only preliminary conclusions based on a visual inspection of the unsteady pressure signals. A rigorous analysis, based on ensemble averaging and a frequency content of the experimental pressure data will reveal more details and reach reliable conclusions about forcing effects on unsteady pressures in a cascade of transonic fan airfoils.

Once-per-period and accelerometer data

The oscillating blade experiences variable acceleration. In an ideal case, the acceleration will follow a periodic sine function with zero values for the blade passing through the ‘zero’ angle position (it is at *30.0 dg* angle). Consequently, measuring the acceleration function, synchronized with the pressure data acquisition, it should be possible to allocate easily the instant of the blade ‘zero’ angle in the pressure data history. An accelerometer cannot be placed on the blade while acquiring pressures because even the miniature accelerometers are ‘bulky’ and the blade and cascade flow patterns would be severely distorted. An attempt was made to measure the blade acceleration by placing two accelerometers out of the cascade flow, an arm that was attached to the blade-tip shaft that protruded through the cascade wall. The arrangement is shown in Fig. 7.6. Two Entran accelerometers model EGA-5000 were used, but eventually only one accelerometer eventually worked. The span of the arm modeled the blade chord. The accelerometer was placed *40.2 mm* of the axis of the blade shaft. The calculated

maximum amplitude (at *±0.6 dg* angle), velocity (at *0.0 dg* angle) and acceleration (at *±0.6 dg* angle) for the transducer location are given in Tab. 7.1 for the range of oscillation frequencies from *200 Hz* to *500 Hz*. The accelerometer data recorded are shown in Fig. 7.7 together with the OPP signal. The figures show raw signals converted to 'g-values' ($g = 9.81\ m/s^2$) using the manufacturer stated sensitivity of *0.061 mV/g*.

A first glance at the accelerometer data reveals that there are severe problems. It must be stressed here that the intention behind this exercise was to back up the OPP signal in determining the blade 'zero' angle using accelerometer signal, and not to measure accurately the blade acceleration. The accelerometers were used without prior calibration just to indicate the shape of the acceleration signal. The first problem is the level of the maximum accelerations that seems to be on the order of *60g* to *70g* for oscillation frequencies up to *400 Hz*, which is wrong. In particular for frequencies of *200 Hz* and *300 Hz*, this is not even possible because the maximum level should be *17g* and *38g*, respectively (see Tab. 7.4). The reason for that might be in the range of the available transducer, which was *±5000g*. Even for a very high accelerometer accuracy of 1.0 %, the maximum acceleration levels for *200 Hz* and *300 Hz* are below the accuracy threshold. For frequencies *400 Hz* and *500 Hz*, the recorded maximum acceleration reaches occasionally levels close to the expected values. The second problem is the shape of the acceleration function. Surprisingly, for the *200 Hz* case, for which the maximum acceleration level is not reliable, the acceleration trace shape is quite clean. As indicated by the arrows in Fig. 7.7a, the zero acceleration instants happen about *0.75 ms* past the once-per-period peaks, which is close to the value of *1.08 ms* as determined from the static conditions described in Fig. 3.3. For the frequencies above *200 Hz* the acceleration function is heavily contaminated with higher frequencies that do not allow determining instants of zero acceleration levels with an acceptable accuracy. The reason for this high-frequency contamination might be slipping of the arm on the shaft during oscillation, and insufficient arm stiffness that allow arm own oscillations (flexing). Both these problems will be addressed in the second phase of the flutter experiments that will be carried out for larger oscillation amplitudes.

8. Lessons learned

The following lessons were learned from the first phase of experiments on transonic flutter:

Transducer leads. Four blades instrumented with 60 miniature Kulite pressure transducers were available at the onset of the research work. Unfortunately, half of the transducers were lost within first several test runs. The primary reason for it was cracking of transducer wires at the backface of the blade shaft. The thin transducer wires pass through the blade shaft and are spliced to thicker wires. The thin wires are cemented in the blade shaft. The thicker wires are routed through the cam box to get the transducer signals out of the cascade. The arrangement was illustrated in Figs. 2.7 and 2.8. Each transducer has four wires. If a single wire cracks, the transducer is lost. All damage to the wires happened just at the backface of the blade shaft. It is not feasible to repair individual leads cemented in the blade shaft. A better solution would be to enlarge the cavity in the blade shaft and spliced the fragile Kulite leads to thicker wires ahead of the shaft end, pull the splicing points inside the shaft and cement the thicker wires in the shaft end. This arrangement will give chance to repair broken wires by removing the cement plug, pull the thin wire out of the shaft, and redo splicing. Unfortunately, this is a very costly solution because the entire blade (15 transducers) must be reinstrumented with a new batch of transducers.

Signal contamination. For operation reasons, the signal conditioners had to be located in the control room and not in the test cell. Low voltages from Kulite transducers were carried over a distance of *12 m*. All precautions were made to eliminate ground loops and properly shield all signal carrying wires, nevertheless some signals exhibited contamination and spurious spikes that could not be associated with flowfield pressure changes. A better solution would be to use newly available NI signal conditioner / excitation modules that can be remotely controlled by the UDAS and can be located just outside of the cam box, very close to transducers. This will minimize the length of cables carrying low voltages and minimize possibility of outside effects on transducer signal quality. However, this solution will also be somewhat costly.

Kulite calibration. The adopted procedure for Kulite transducers seemed to be satisfactory as demonstrated by relatively very good agreements of Kulite DC pressure levels with data from conventional static taps (see Fig. 3.5 as an example). As described in Chapter 4, zeros for all Kulite transducers were recorded just prior commencement of each test group. These readings, instantaneous zero offsets, respectively their differences from the zero offset recorded during the last previous Kulite calibration, were used for data correction for transducer zero drift. In future experiments, testing will be interrupted every two or three hours to allow for more frequent readouts of Kulite instantaneous zeros to further improved the accuracy of DC pressure levels measured with Kulite transducers.

Once-per-period signal. The OPP pickup worked reliably. The only inconvenience was of the current arrangement was that the pickup holder did not allow for position adjustment along the circumference of the hexagon cam and therefore the OPP signal could not be aligned with the 'zero' blade angle already on the hardware side but it had to be aligned during the data postprocessing (as explained in Fig. 3.3). A small design change in the layout of the OPP holder will eliminate this inconvenience for the future testing.

Accelerometer data. The accelerometer arm must be stiffer to avoid arm oscillations in order to record blade acceleration more reliably. This is even more true amplitude of blade oscillations larger than *0.6 dg* because a significant increase in blade-tip acceleration. The easiest way will be to shorten the arm to a minimum length that will still allow mounting an accelerometer. The accelerometer will not measure now the blade tip acceleration but acceleration at a smaller radius. Because the blade is assumed to be sufficiently rigid, the instants of zero acceleration and blade-zero angle should be still identical. Smaller peak acceleration levels, experienced by the accelerometer will also relieved problems with breaking the accelerometer output leads. Further, more sensitive accelerometers can be used. The range of accelerometer used and the expected range of measured acceleration levels must be matched better than was the case o small amplitude oscillations.

ESCORT/USDA synchronization. Cascade steady data and facility data are acquired by NASA GRC labwide system ESCORT. The unsteady data are acquired using a facility dedicated unsteady data acquisition system (UDAS). At present, these two systems are completely independable without means of mutual communication. All data transfer between the ESCORT and UDAS is done only during the postprocessing phase. It would ease the operation of the test facility and simplify the postprocessing procedures if ESCORT data, relevant to the cascade steady state operation, were synchronized with the data acquisition using UDAS and the these ESCORT experimental data stored concurrently in a suitable form in the USDA data files.

Implication at least some of the above stated suggestions will improve quality and reliability of the pressure unsteady data that will be acquired in the follow up phase of the stall flutter experiment for blade oscillations at large amplitudes.

References

1.1 Buffum, D.H., Capece, V.R., King, A.J., and El-Aini, Y.M.: "Oscillating Cascade Aerodynamics at Large Mean Incidence," ASME Paper 96–GT–339; also NASA TM–107247, 1996.

1.2 Buffum, D.H., Capece, V.R., King, A.J., and El-Aini, Y.M.: "Experimental Investigation of Unsteady Flows at Large Incidence Angles in a Linear Oscillating Cascade," AIAA Paper 96–2823; also NASA TM–107283, 1996.

1.3 Buffum, D.H. and Fleeter, S.: "Wind Tunnel Wall Effects in a Linear Oscillating Cascade," NASA TM–103690, 1991.

1.4 Ott, P., Norryd, M., and Bölcs, A.: "The Influence of Tailboards on Unsteady Measurements in a Linear Cascade," ASME Paper 98–GT–572, 1998.

1.5 Buffum, D.H. and Fleeter, S.: "Investigation of Oscillating Cascade Aerodynamics by an Experimental Influence Coefficient Technique," NASA TM–101313, 1988.

2.1 Boldman, D.R. and Buggele, A.E.: “Wind Tunnel Tests of a Blade Subjected to Midchord Torsional Oscillations at High Subsonic Stall Flutter Conditions,” NASA TM–78998, 1978.

2.2 Shaw, L.M., Boldman, D.R., Buggele, A.E., and Buffum, D.H.: “Unsteady Pressure Measurements on a Biconvex Airfoil in a Transonic Oscillating Cascade,” *Journal of Engineering for Gas Turbines and Power*, Vol. 108, pp. 53–59, 1986.

2.3 Lepicovsky, J., McFarland, E.R., Chima, R.V, and Wood, J.R.: “On Flowfield Periodicity in the NASA Transonic Flutter Cascade, Part I—Experimental Study,” ASME Paper 2000–GT–0572, 2000.

2.4 Chima, R.V, McFarland, E.R., Wood, J.R., and Lepicovsky, J.: “On Flowfield Periodicity in the NASA Transonic Flutter Cascade, Part II—Numerical Study,” ASME Paper 2000–GT–0573, 2000.

2.5 Lepicovsky, J., McFarland, E.R., Chima, R.V, and Wood, J.R.: “On Flowfield Periodicity in the NASA Transonic Flutter Cascade,” Journal of Turbomachinery, Vol. 123, pp. 501–509, 2001.

3.1 Fronek, D.L., Setter, R.N., Blumenthal, P.Z., and Smally, R.R.: “A Distributed data Acquisition System for Aeronautics Test Facilities,” NASA TM–88961, 1987.

4.1 Lepicovsky, J., Chima, R.V., Jett, T.A., Bencic, T.J., and Weiland, K.E.: “Investigation of Flow Separation in a Transonic-Fan Linear Cascade Using Visualization Methods,” International Symposium on Flow Visualization, Paper 335, 2000.

5.1 Gerolymos, G.A.: “Periodicity, Superposition, and 3D Effects in Supersonic Compressor Flutter Aerodynamics,” *International Journal of Turbo and Jet Engines,* Vol. 7, pp. 143–152, 1990.

5.2 Buffum, D.H. and Fleeter, S.: "Oscillating Cascade Aerodynamics by an Experimental Influence Coefficient Technique," *AIAA Journal of Propulsion and Power*, Vol. 6, No. 5, pp. 612–620, 1990.

5.3 Bolcs, A., Fransson, T.H. and Schlafi, D.: "Aerodynamic Superposition Principle in Vibrating Turbine Cascades," *AGARD–CPP–468/469*, pp. 5–1 – 5–19, 1989.

5.4 Fransson, T.H.: "Analysis of Experimental Time-Dependent Blade Surface Pressures from an Oscillating Turbine Cascade with the Influence-Coefficient Technique," *ASME Paper No*. 90–GT–225, 1990.

5.5 Smith, S.N.: "Discrete Frequency Sound Generation in Axial Flow Turbomachines," Aeronautical Research Council Reports and Memoranda No. 3709, 1973.

6.1 McFarland, E.R.: “A Rapid Blade-to-Blade Solution for Use in Turbomachinery Design,” *Journal of Engineering for Power,* Vol. 106, pp. 376–382, 1984.

6.2 McFarland, E.R.: “An Integral Equation Solution for Multistage Turbomachinery Design Calculations,” ASME paper 93–GT–41, 1993.

6.3 Chima. R.V.: “Explicit Multigrid Algorithm for Quasi-Three-Dimensional Viscous Flows in Turbomachinery,” *AIAA Journal propulsion and Power,* Vol. 3, No. 5, pp 397–405, 1987.

6.4 Chima, R.V.: “Calculation of Tip Clearance Effects in a Transonic Compressor Rotor,” ASME Paper 96–GT–114, Also NASA TM–107216, 1996.

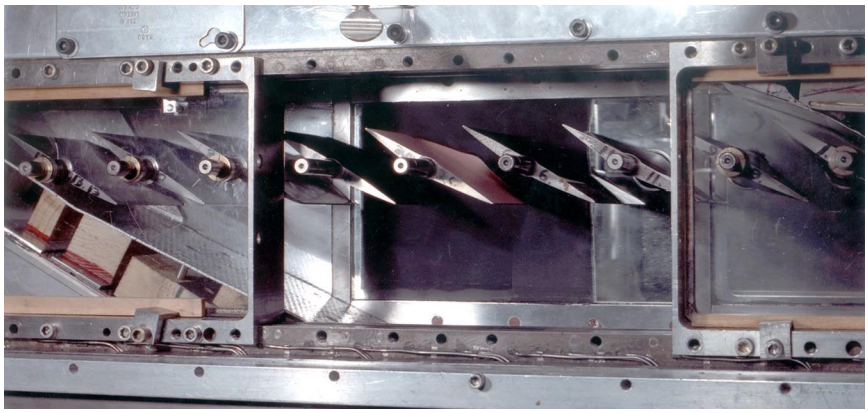

Fig. 1.1 Test section of the NASA Transonic Flutter Cascade.

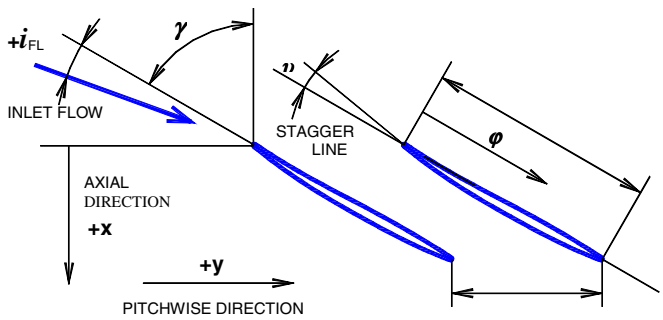

Fig. 1.2 Airfoil and cascade coordinate system.

Blade chord,	C	89.2 mm
Leading edge camber angle,	υ	29.5 dg
Maximum thickness,	t_{max}	0.048 C
Location of maximum thickness,	φ_{max}	0.625 C
Stagger angle,	γ	60.0 dg
Number of blades in the cascade		9
Blade pitch,	S	58.4 mm
Cascade solidity,	C/S	1.53
Pitching axis,	φ_{ax}	0.5 C
Blade height,	h	95.9 mm

Tab. 1.1 Airfoil and cascade parameters.

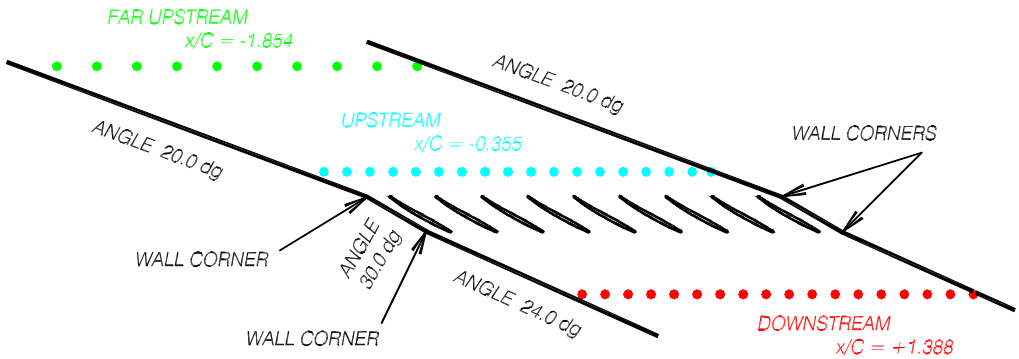

Fig. 2.1. Cascade configuration *C_20.0 / 24.0.*

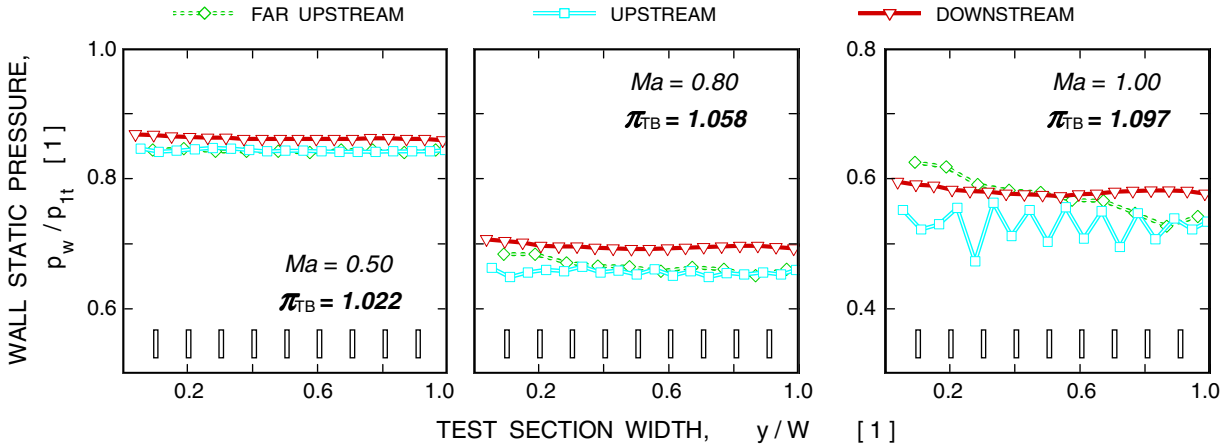

Fig. 2.2. Wall static pressure distributions for cascade configuration *C_20.0 / 24.0.*

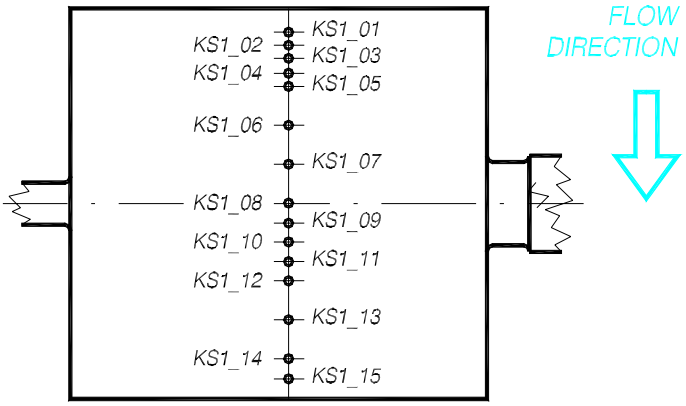

BLADE KS1

Instrumented suction surface

Blade height 95.9 mm
Height of ports 45.7 mm (from blade root)

Blade chord 89.4 mm

Port 1 5.4 mm (6.0%)	Port 6 26.8 mm (30.0%)	Port 11 58.0 mm (64.9%)
Port 2 8.5 mm (9.5%)	Port 7 35.6 mm (39.8%)	Port 12 62.4 mm (69.8%)
Port 3 11.6 mm (13.0%)	Port 8 44.6 mm (49.9%)	Port 13 71.3 mm (79.8%)
Port 4 14.8 mm (16.6%)	Port 9 49.2 mm (55.0%)	Port 14 80.2 mm (89.7%)
Port 5 17.9 mm (20.0%)	Port 10 53.5 mm (59.8%)	Port 15 84.7 mm (94.7%)

Fig. 2.3 Typical location of pressure ports on the blade suction side.

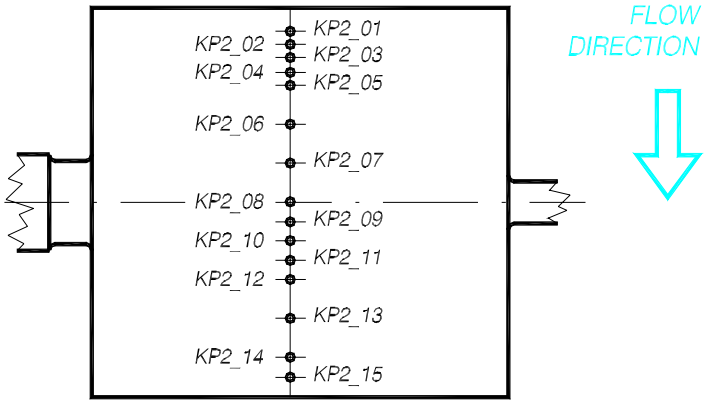

BLADE KP2

***Instrumented pressure* surface**

Blade height 95.8 mm
Height of ports 45.9 mm (from blade root)

Blade chord 89.3 mm

Port 1 5.4 mm (6.1%)	Port 6 26.7 mm (29.9%)	Port 11 57.9 mm (64.8%)
Port 2 8.4 mm (9.4%)	Port 7 35.6 mm (39.9%)	Port 12 62.3 mm (69.8%)
Port 3 11.7 mm (13.1%)	Port 8 44.5 mm (49.8%)	Port 13 71.2 mm (79.7%)
Port 4 14.8 mm (16.6%)	Port 9 49.1 mm (55.0%)	Port 14 80.1 mm (89.7%)
Port 5 17.8 mm (19.9%)	Port 10 53.4 mm (59.8%)	Port 15 84.7 mm (94.6%)

Fig. 2.4 Typical location of pressure ports on the blade pressure side.

Fig. 2.5 EDM electrode and grooved blade.

Fig. 2.6 Blades prepared for transducer insertion.

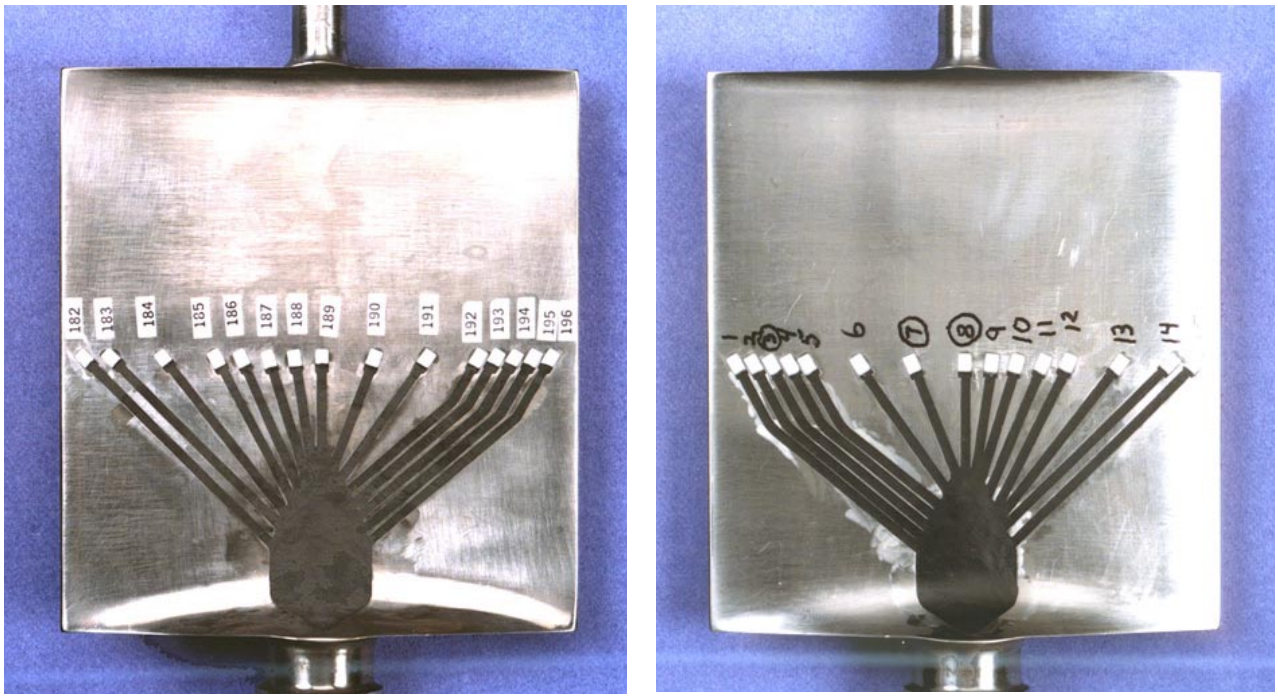

Fig. 2.7 Blades instrumented with Kulite transducers.

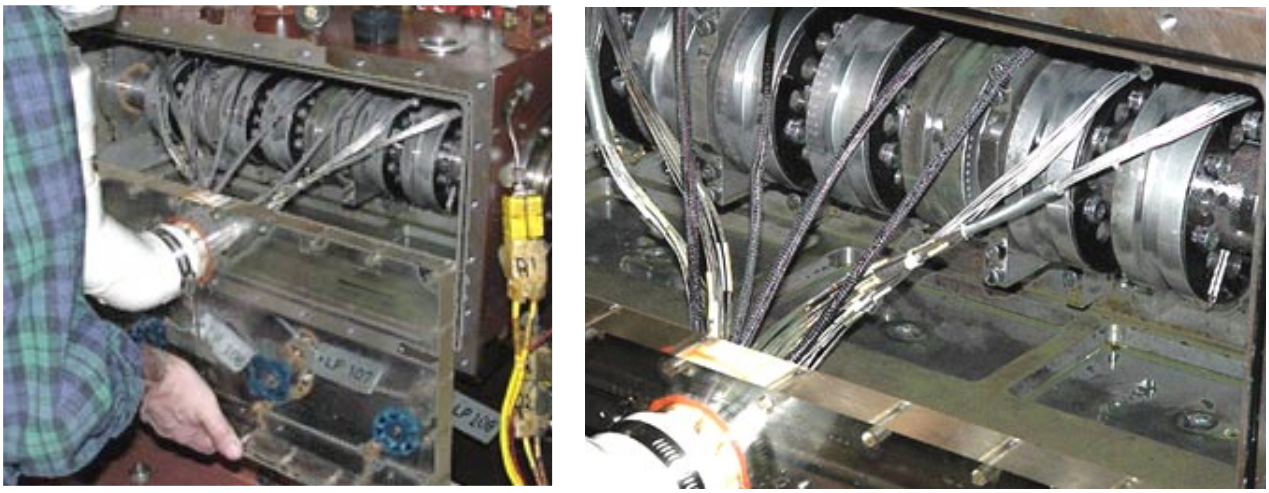

Fig. 2.8 Open cam box routing of transducers leads.

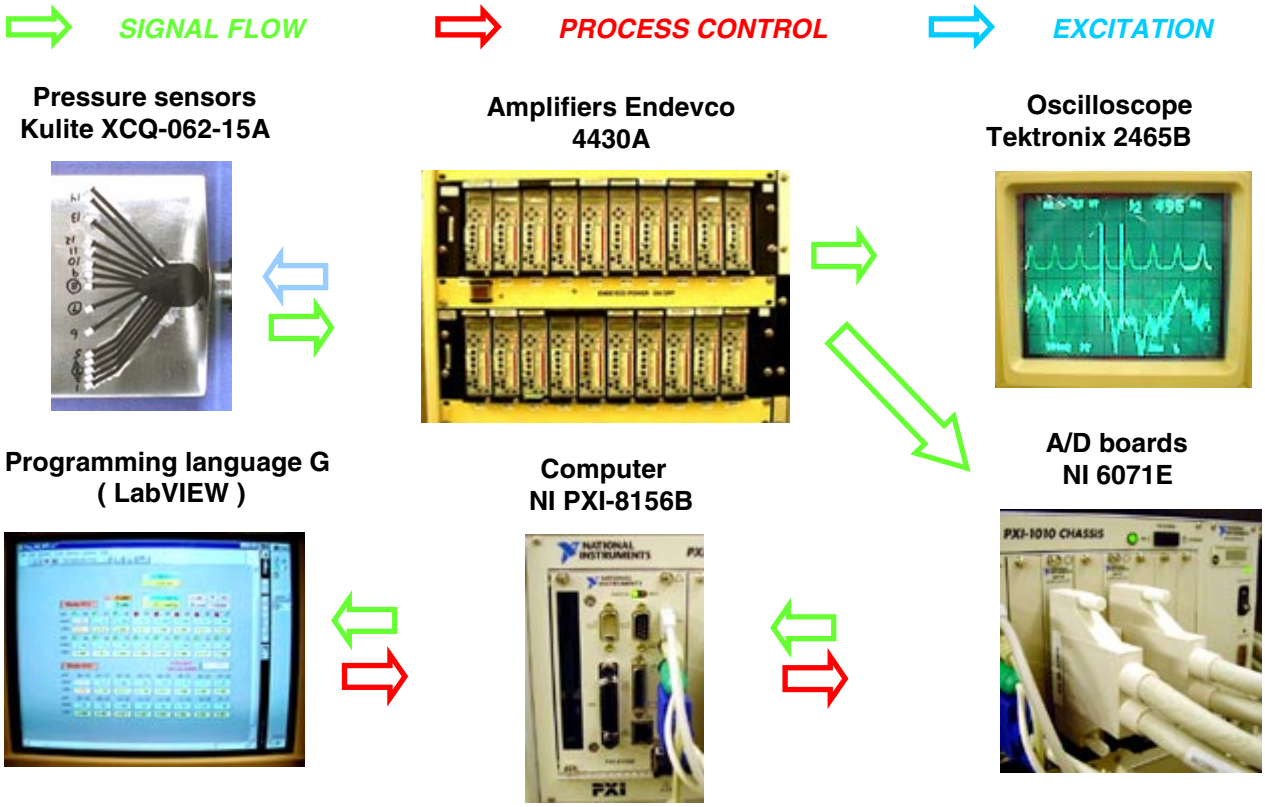

Fig. 3.1 Unsteady data acquisition system.

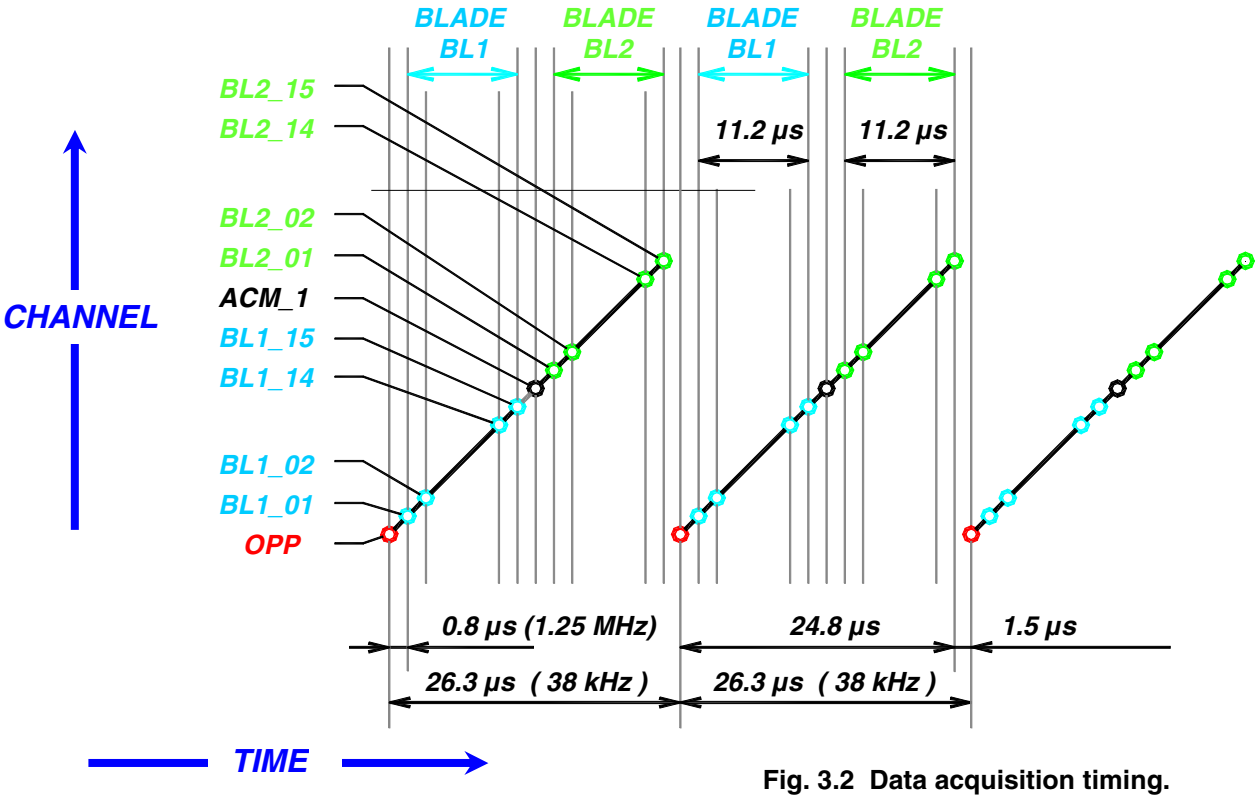

Fig. 3.2 Data acquisition timing.

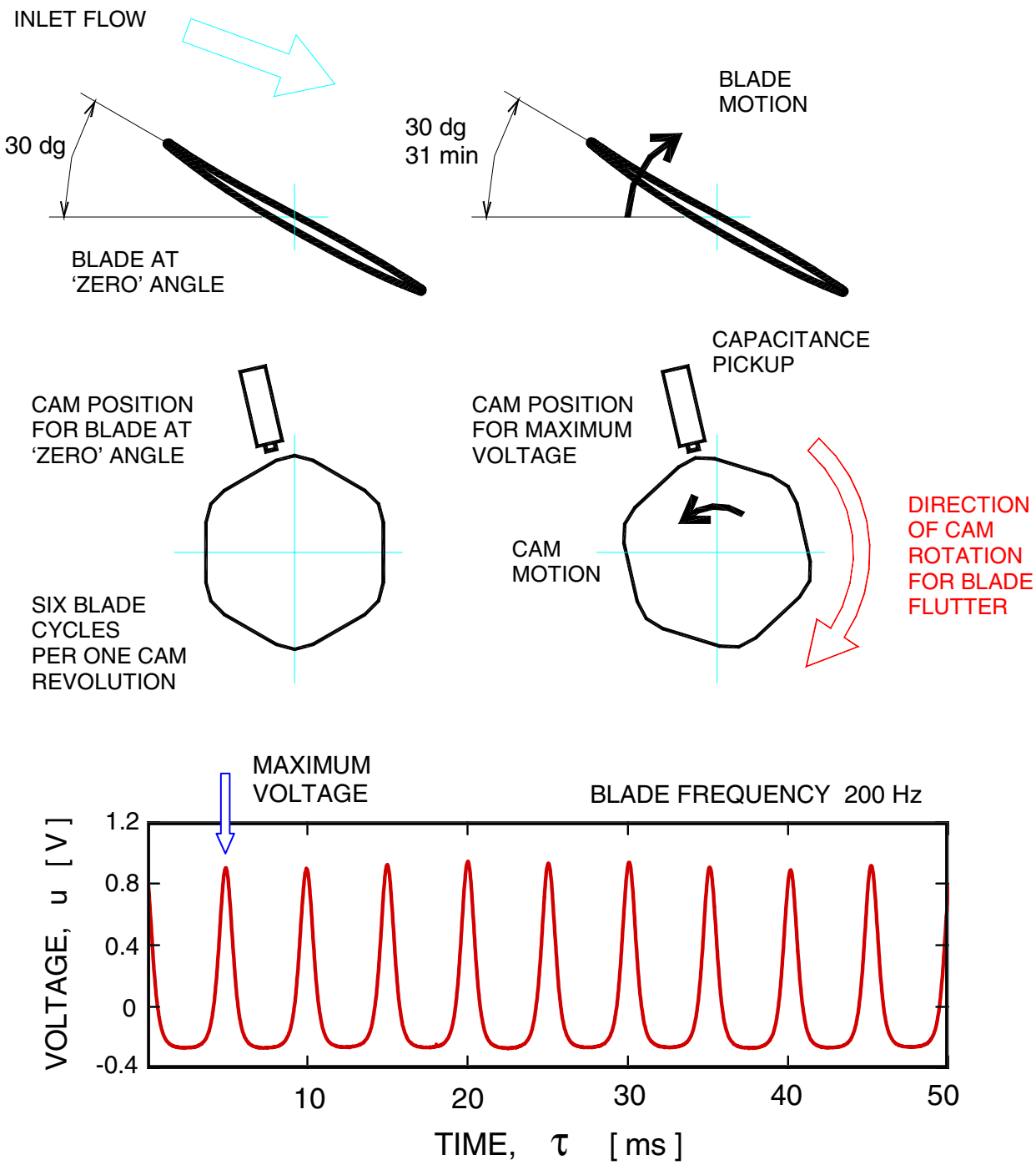

Fig. 3.3 Blade 'zero' angle position in the signal time history.

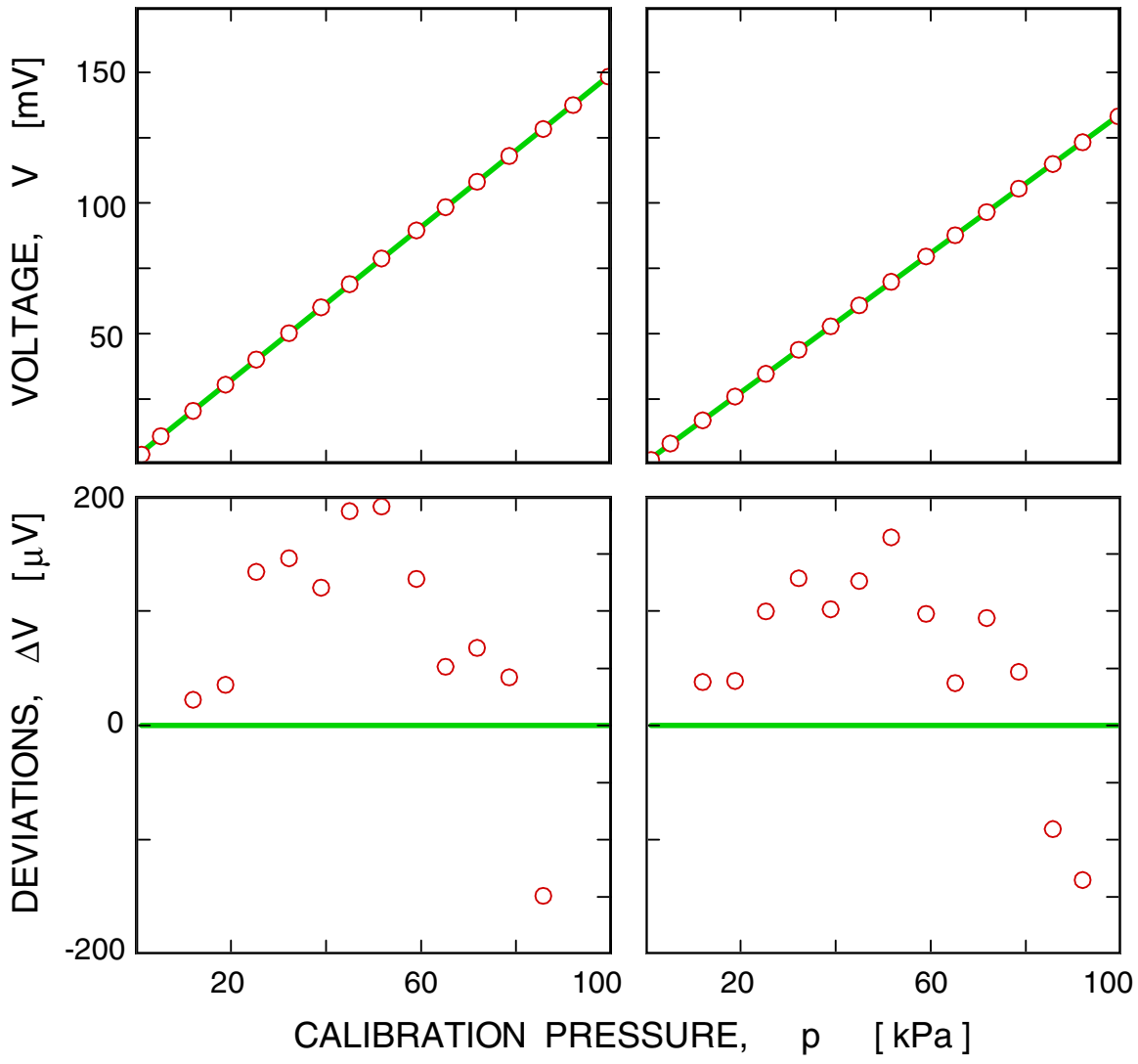

Fig. 3.4 Typical Kulite calibration results.

Blade KP1		07-Sep-00	24-Oct-00	25-Jan-01	20-Mar-01
Port 01		KP1_01	KP1_02	KP1_03	KP1_04
slope	[mV/kPa]	1.248	1.251	1.247	1.247
y_0	[mV]	1.35	1.43	1.32	1.28
s_dev	[mV]	188.8	222.8	245.9	473.7
Port 02					
slope	[mV/kPa]	1.612	1.612	1.611	1.609
y_0	[mV]	2.98	3.03	3.03	2.51
s_dev	[mV]	294.9	340.5	351.4	650.2
Port 04					
slope	[mV/kPa]	1.262	1.265	1.261	1.260
y_0	[mV]	-3.41	-3.60	-3.80	-3.98
s_dev	[mV]	199.8	244.4	250.6	485.4
Port 05					
slope	[mV/kPa]	1.477	1.478	1.476	1.475
y_0	[mV]	5.72	5.50	4.70	4.20
s_dev	[mV]	274.9	306.4	309.3	582.2
Port 06					
slope	[mV/kPa]	1.466	1.470	1.468	1.468
y_0	[mV]	2.83	2.64	2.72	2.40
s_dev	[mV]	259.4	295.5	290.3	571.6
Port 09					
slope	[mV/kPa]	1.460	1.464		
y_0	[mV]	5.65	5.72		
s_dev	[mV]	196.7	231.5		
Port 10					
slope	[mV/kPa]	1.333	1.336	1.335	1.341
y_0	[mV]	0.77	0.85	0.60	-0.23
s_dev	[mV]	214.6	248.0	253.7	510.1
Port 11					
slope	[mV/kPa]				1.916
y_0	[mV]				3.53
s_dev	[mV]				857.9
Port 12					
slope	[mV/kPa]	1.342	1.342	1.344	1.342
y_0	[mV]	0.94	0.48	-2.36	-5.94
s_dev	[mV]	222.3	256.0	266.1	513.8
Port 13					
slope	[mV/kPa]	1.327	1.326	1.323	1.321
y_0	[mV]	2.04	1.86	1.83	1.42
s_dev	[mV]	210.9	246.6	262.6	509
Port 15					
slope	[mV/kPa]	1.372	1.376	1.370	1.369
y_0	[mV]	0.48	0.14	0.29	-0.08
s_dev	[mV]	245.4	290.8	275.8	536.6

Tab. 3.1 Calibration results for blade KP1.

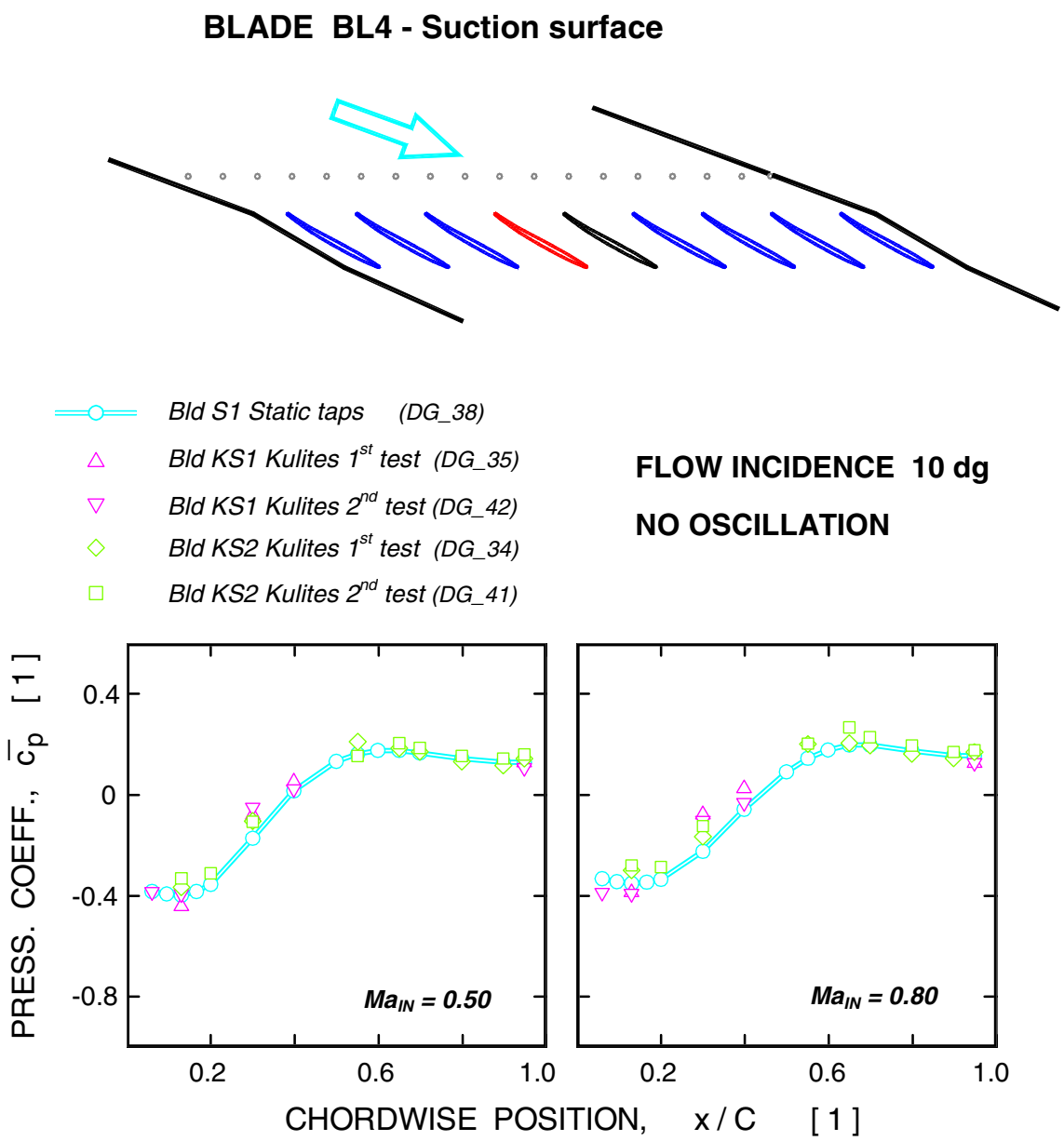

Fig. 3.5 Comparison of static tap data with Kulite average pressure data for suction side of blade BL4.

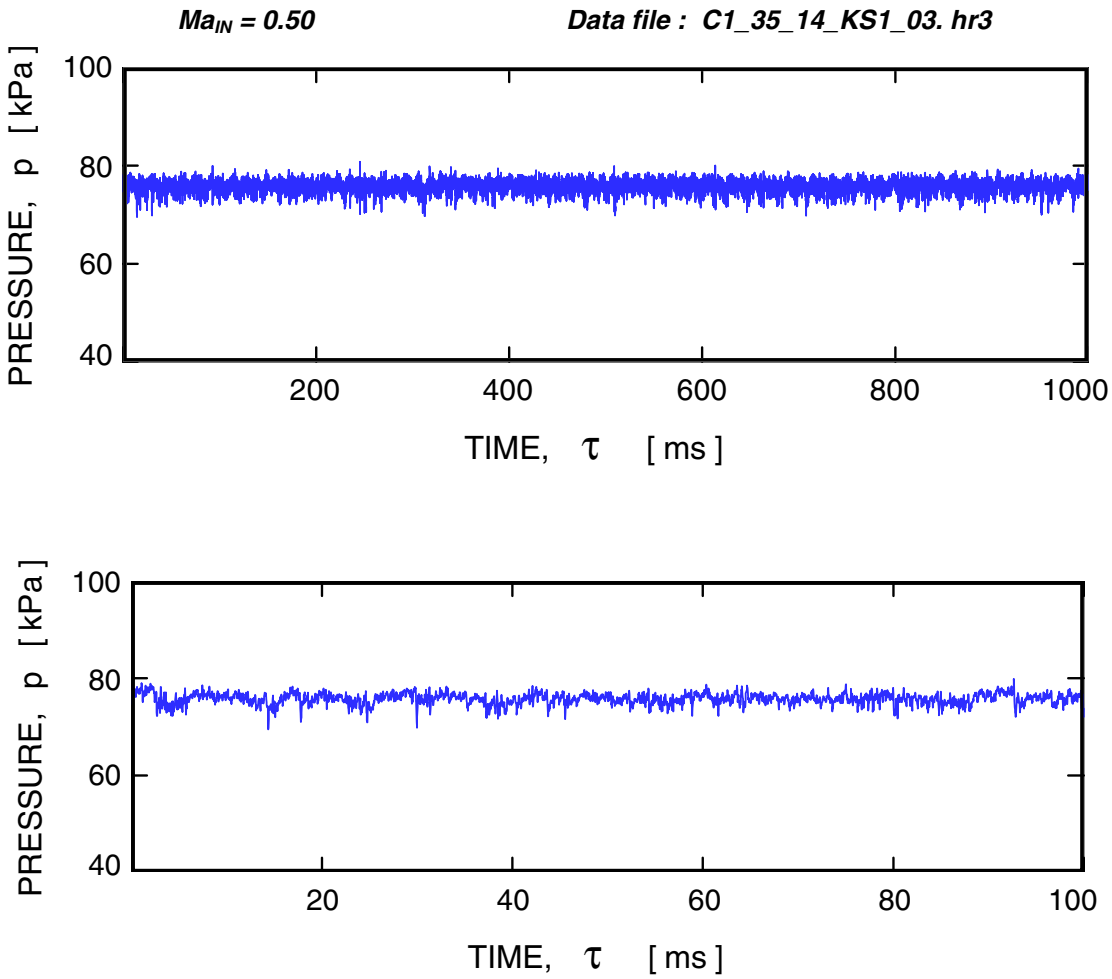

Fig. 4.1 Uncontaminated raw data signal.

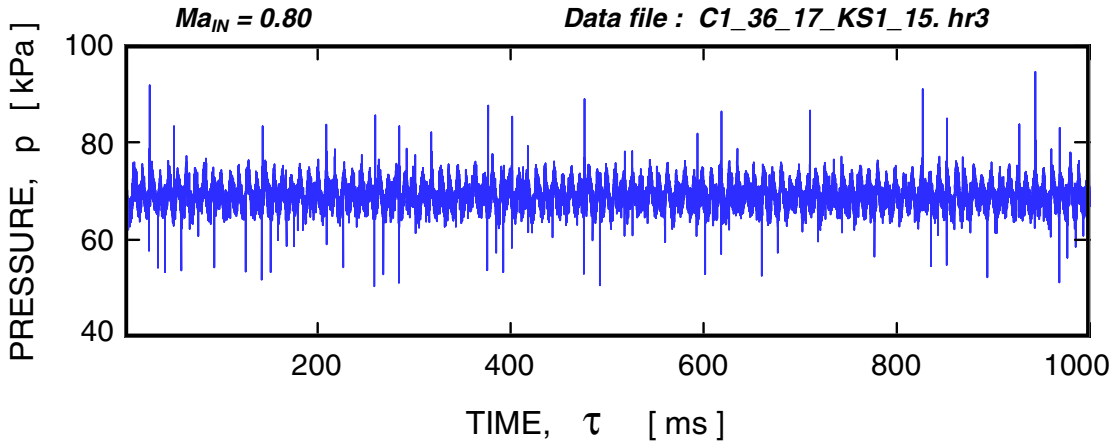

Fig. 4.3a Data signal heavily contaminated by 'single point ' spikes.

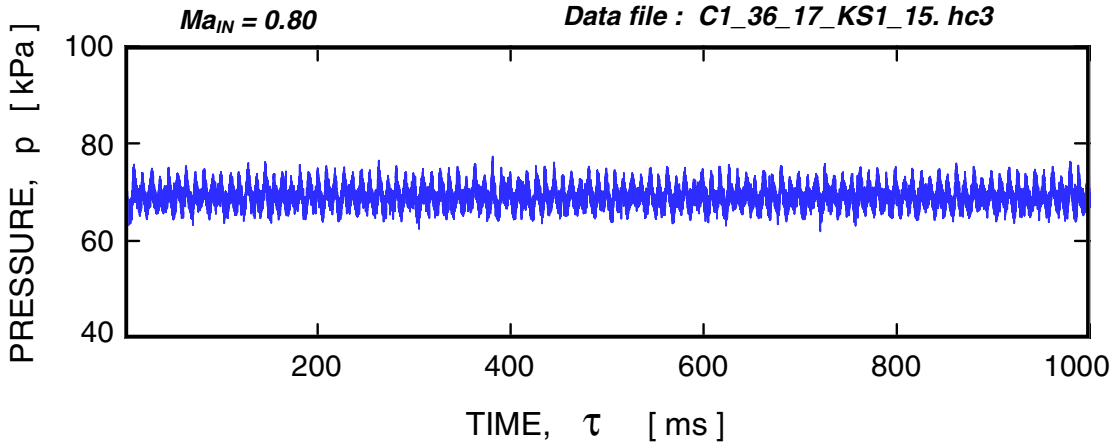

Fig. 4.3b Data signal cleaned by the clipping procedure.

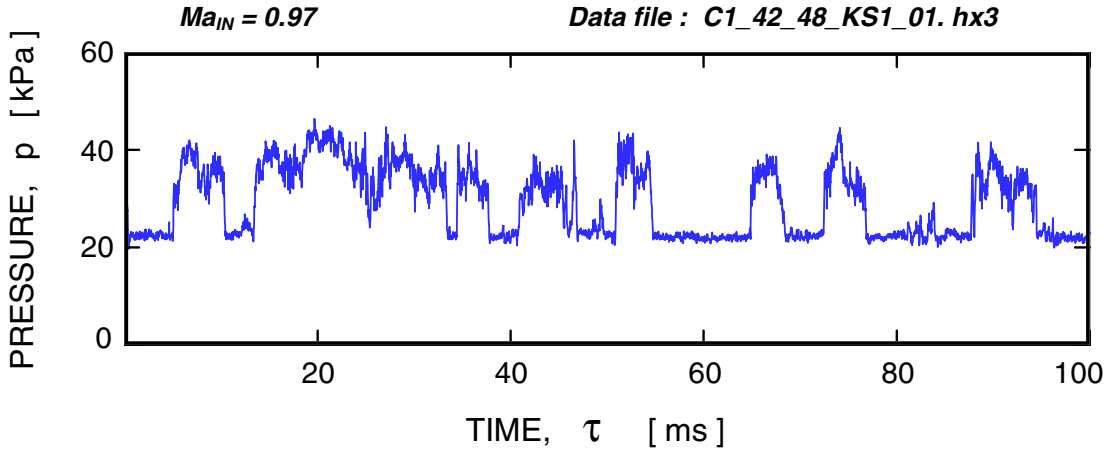

Fig. 4.2 Bistable flow (pressure jumping) in the transonic region.

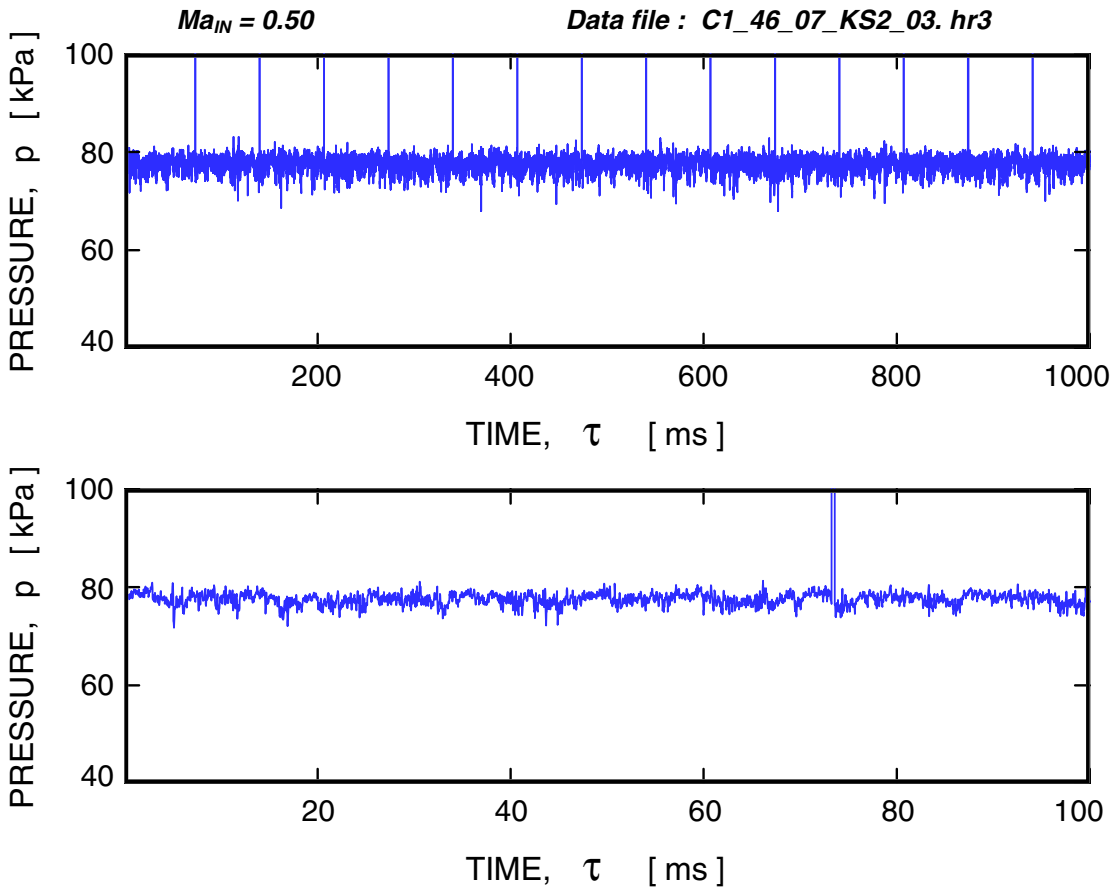

Fig. 4.4 Data signal heavily contaminated by temporarily dropouts (amplifier saturation).

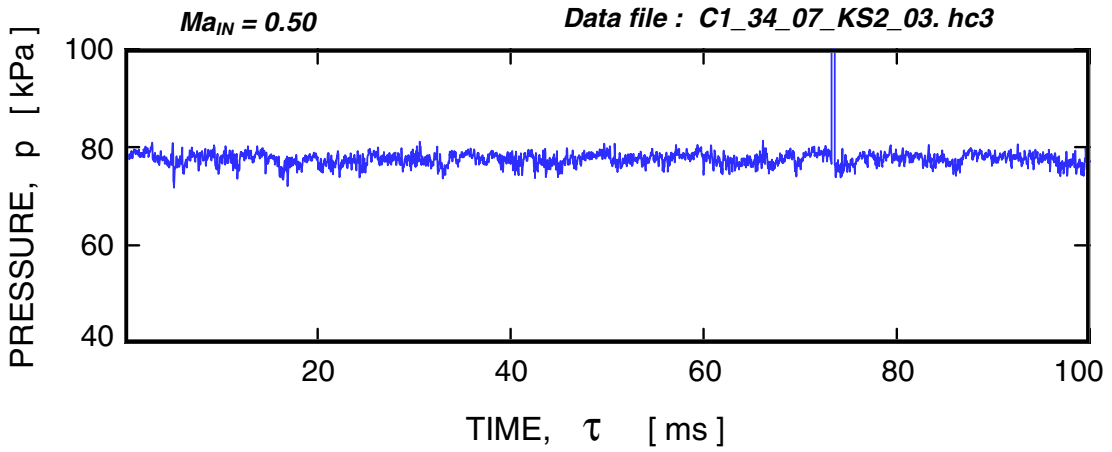

Fig. 4.5 Data signal cleaned by the clipping procedure.

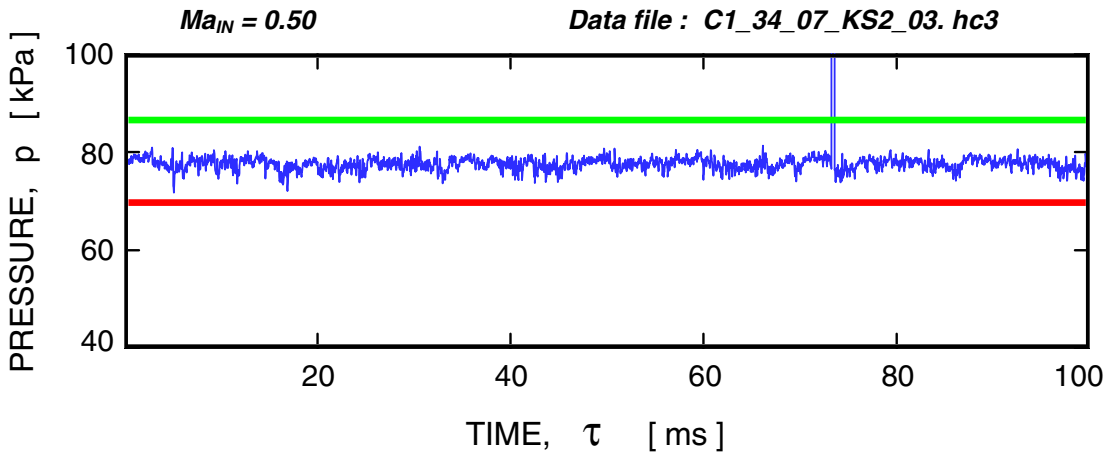

Fig. 4.6 Upper and lower pressure limits.

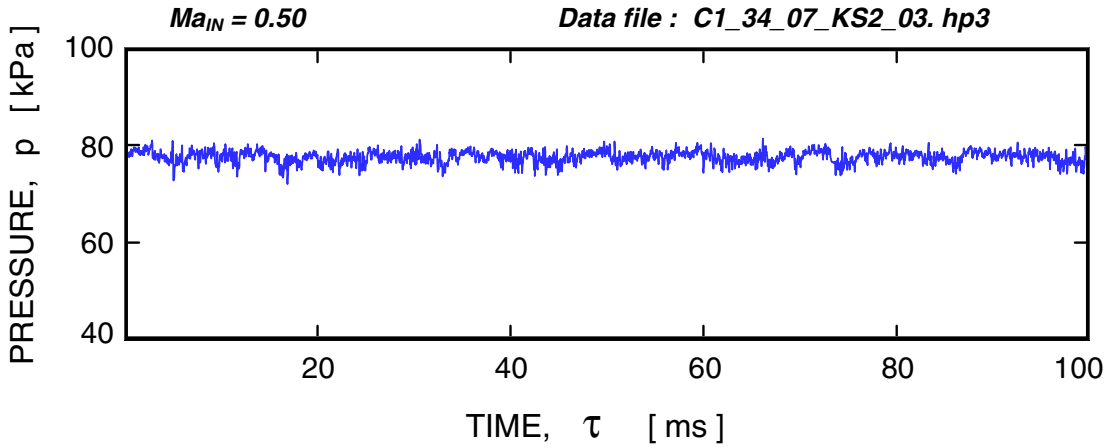

Fig. 4.7 Data signal cleaned by the patching procedure.

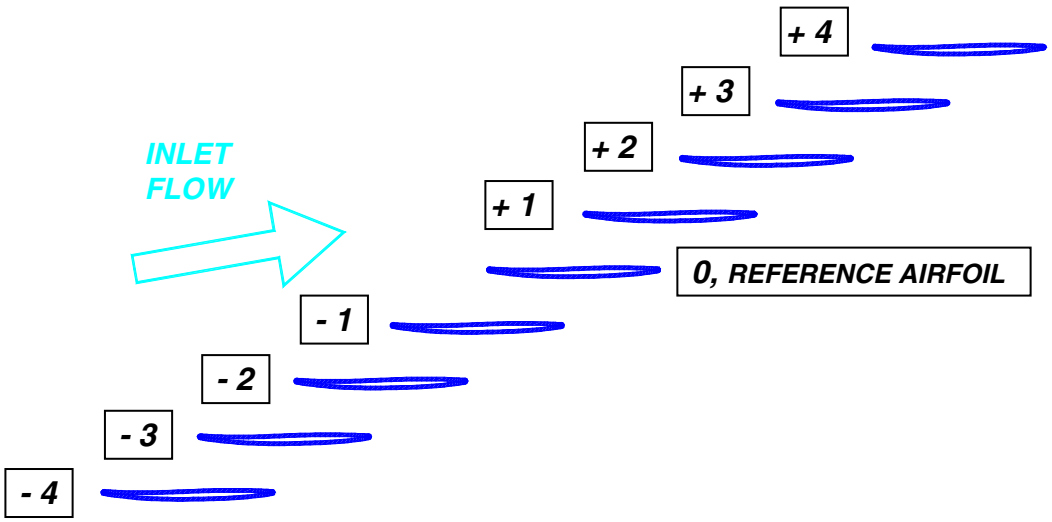

Fig. 5.1 Schematic representation of a cascade of airfoils and the numbering system used for the influence coefficient method.

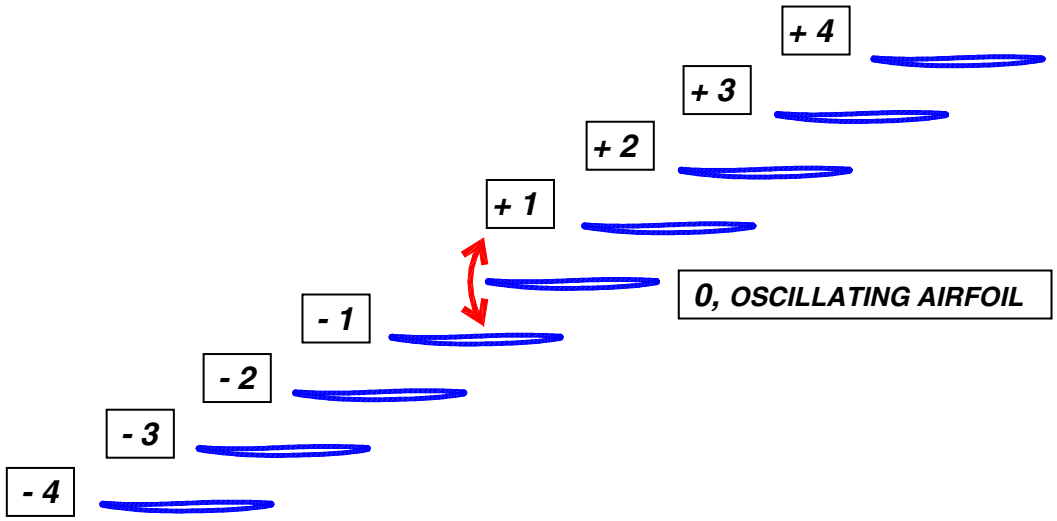

Fig. 5.2 Schematic representation of a cascade of airfoils with the reference airfoil oscillating (n = 0).

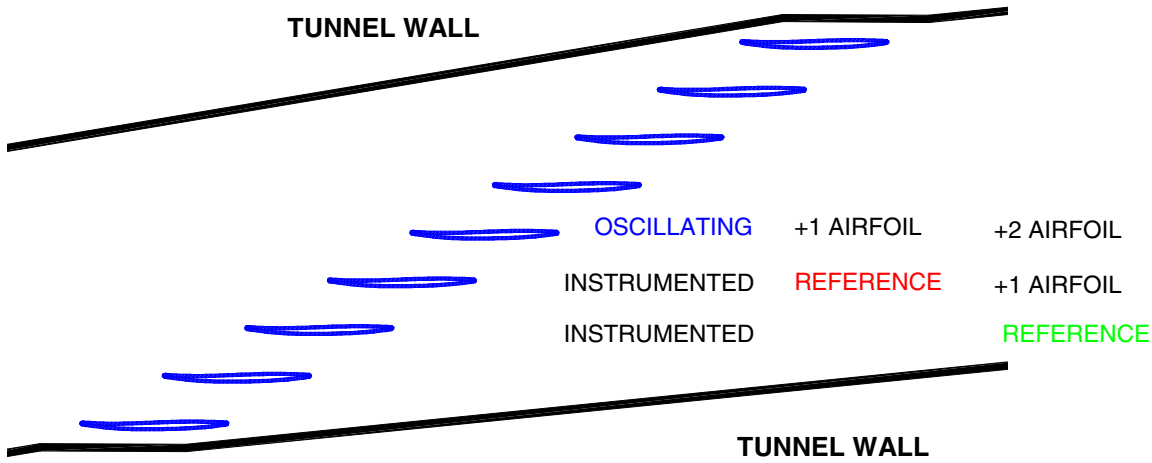

Fig. 5.3 Configuration to measure the +1 and +2 influence coefficients using two instrumented airfoils with the center cascade airfoil oscillating.

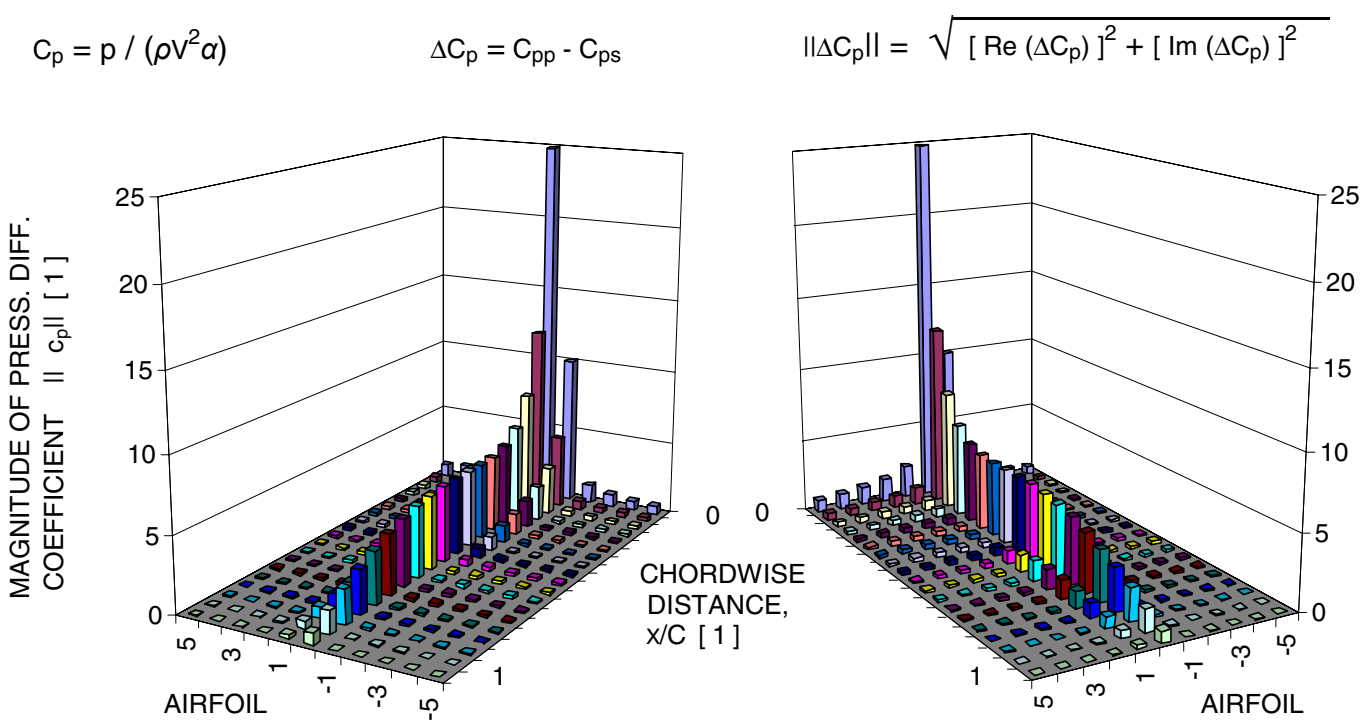

Fig. 5.4 Chordwise distribution of the magnitude of the unsteady pressure difference influence coefficient.

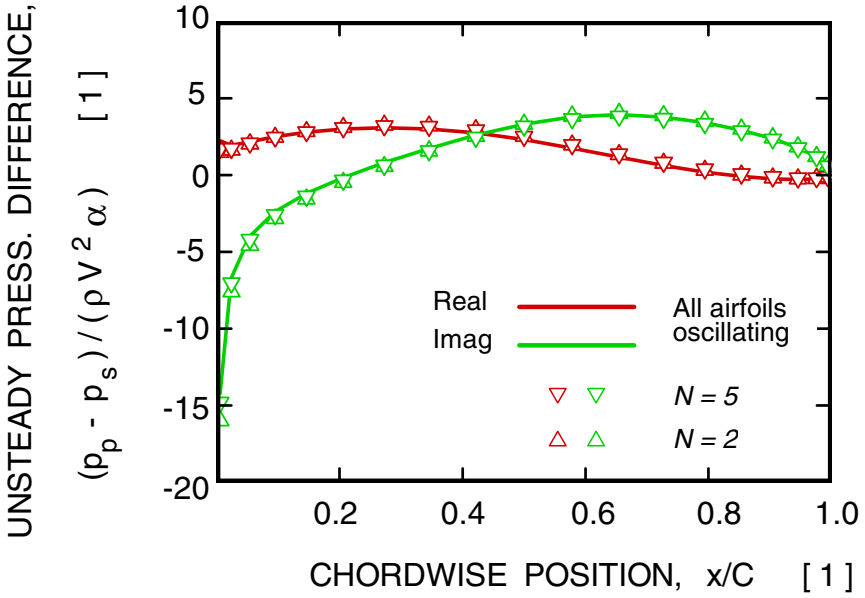

Fig. 5.5. Unsteady pressure difference coefficient distribution for σ = 0 dg, Ma = 0.5, and γ = 60 dg.

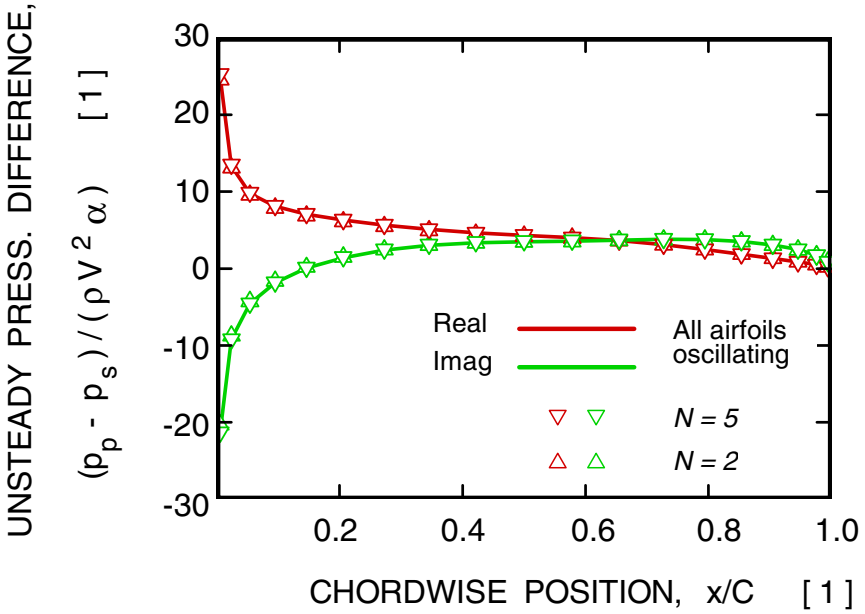

Fig. 5.6. Unsteady pressure difference coefficient distribution for σ = 180 dg, Ma = 0.5, and γ = 60 dg.

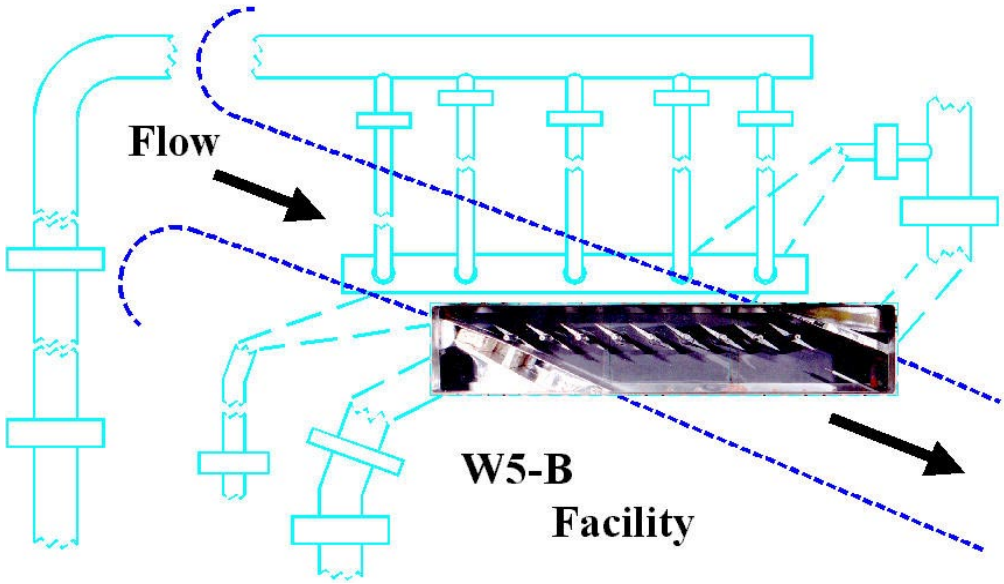

Fig. 6.1a Schematic of the facility with test section shown.

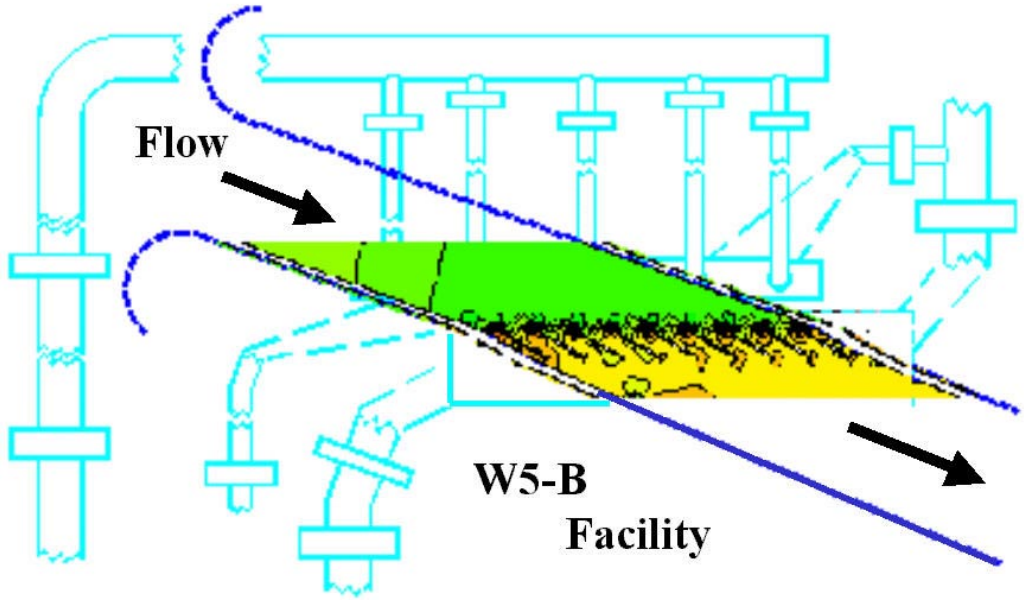

Fig. 6.1b Schematic of the facility with CFD simulation replacing the test section.

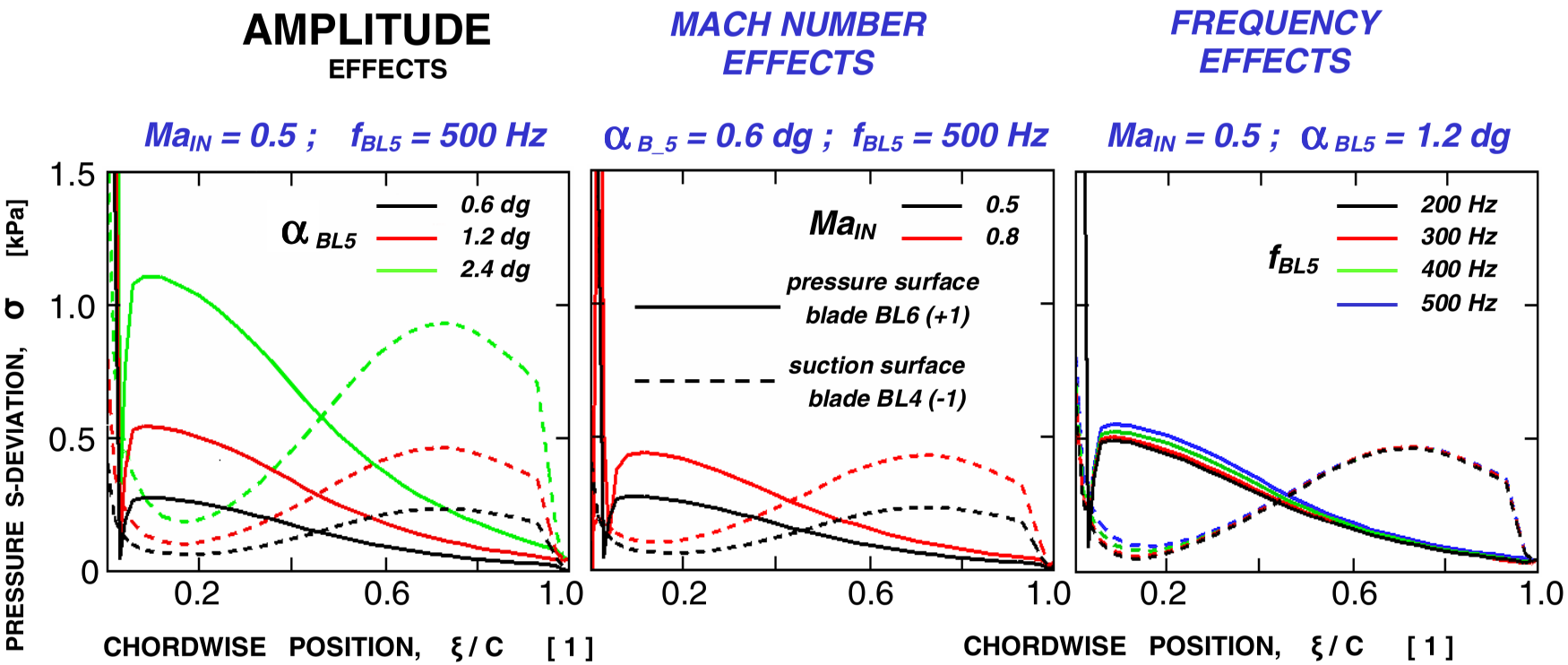

Provides largest impact on loading of adjacent blades. Also, simulation indicates possible wall interference at largest amplitude of 2.4 dg.

Provides significant impact on loading of adjacent blades.

Has little impact on loading of adjacent blades.

Fig. 6.3 Summary of CFD predictions.

incidence angle	10 dg					
oscillation amplitude	0.0 dg					
oscillation frequency	0 Hz					
inlet Mach number	0.40	0.50	0.60	0.70	0.80	0.85
	0.90	0.93	0.95	0.97	0.97	0.99
	1.00	1.01	1.03	1.05	1.10	

Tab. 7.1 Test matrix of nonoscillating blade data.

incidence angle	10 dg			
inlet Mach number	0.5	0.8	1.0	1.1
oscillation amplitude	0.6 dg			
oscillation frequency	200 Hz	300 Hz	400 Hz	500 Hz

Tab. 7.2 Test matrix of oscillating blade data.

Date	BL1	BL2	BL3	BL4	BL5	BL6	BL7	BL8	BL9	Group
09-Mar-00	S1	P1	KS2	KP2	FB	KS1	KP1	S2	P2	33
06-Apr-00	S2	P1	KP2	KS2	FB	S1	KS1	KP1	P2	34
11-Apr-00	S2	KS2	P1	KS1	FB	KP1	S1	KP2	P2	35
20-Apr-00	S2	S1	KS1	KP1	FB	KP2	P1	KS2	P2	36
25-Apr-00	S2	KS1	KP1	S1	FB	KS2	KP2	P1	P2	38
27-Apr-00	S2	KP1	S1	KP2	FB	P1	KS2	KS1	P2	39
04-May-00	S2	KP2	KS2	P1	FB	KS1	KP1	S1	P2	40
10-May-00	S2	S1	KP2	KS2	FB	P1	KS1	KP1	P2	41
16-May-00	S2	KS2	P1	KS1	FB	KP1	S1	KP2	P2	42/43

Tab. 7.3 Blade allocation table.

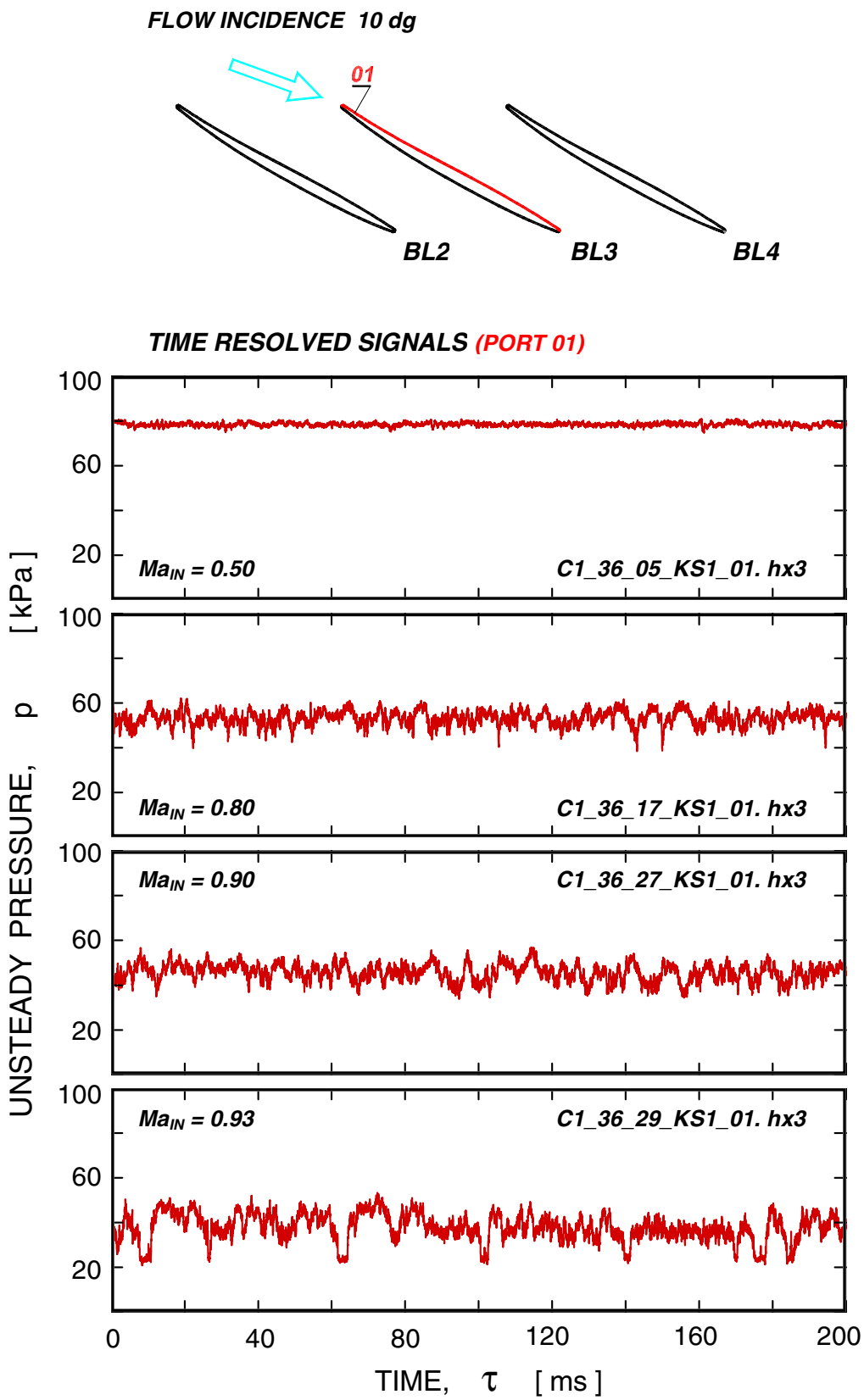

Fig. 7.1a Effects of inlet Mach number on unsteady pressure data.

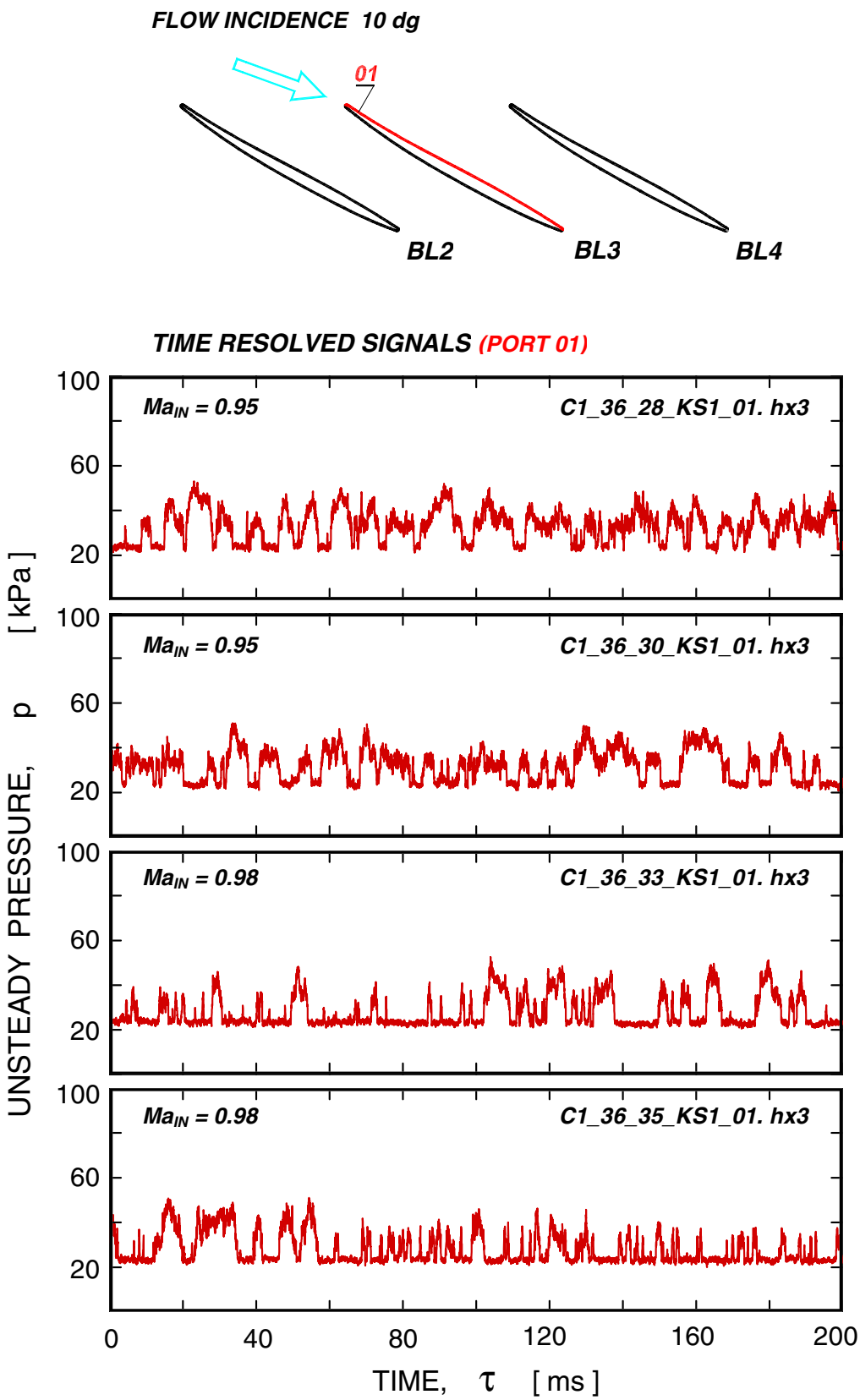

Fig. 7.1b Effects of inlet Mach number on unsteady pressure data.

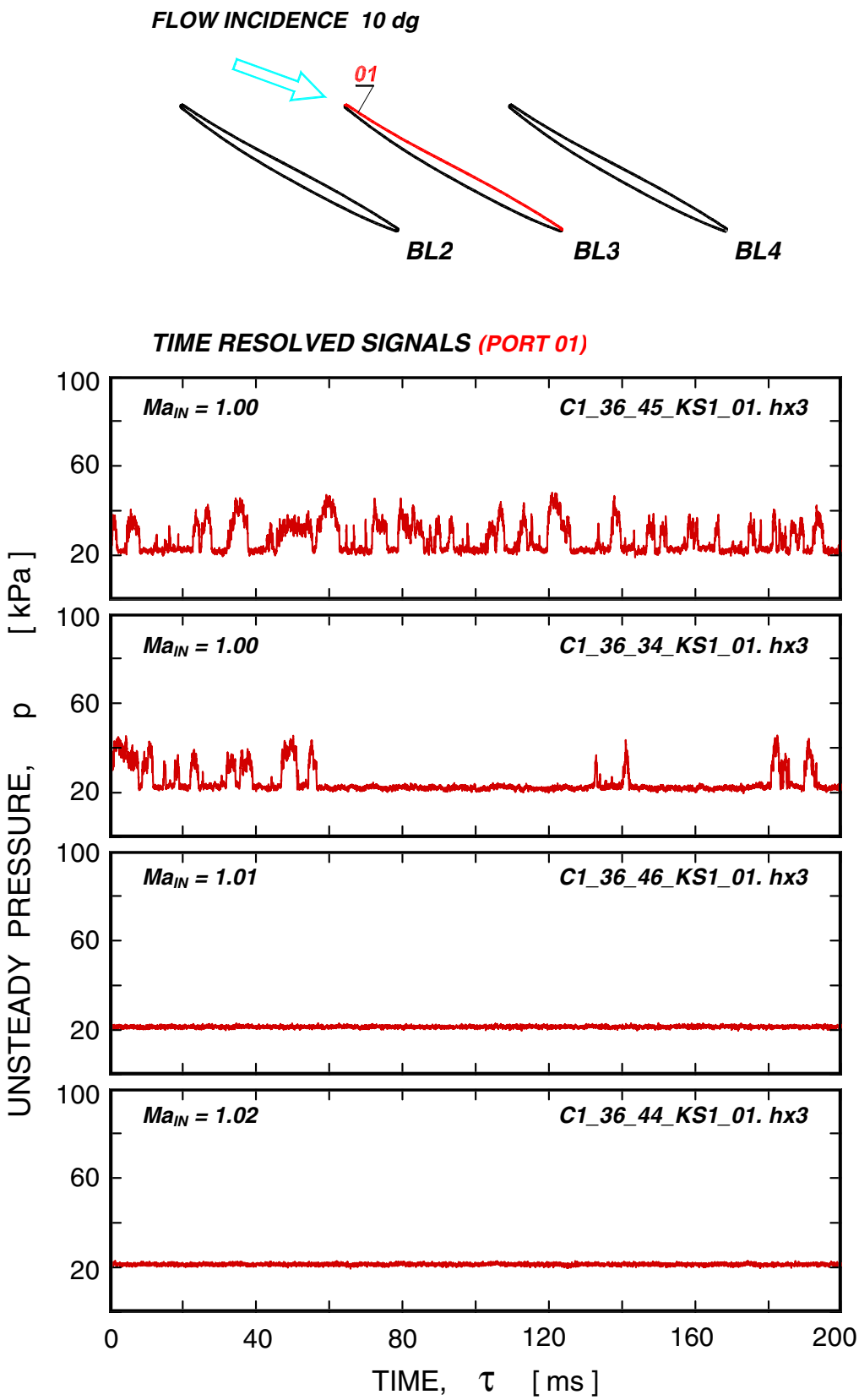

Fig. 7.1c Effects of inlet Mach number on unsteady pressure data.

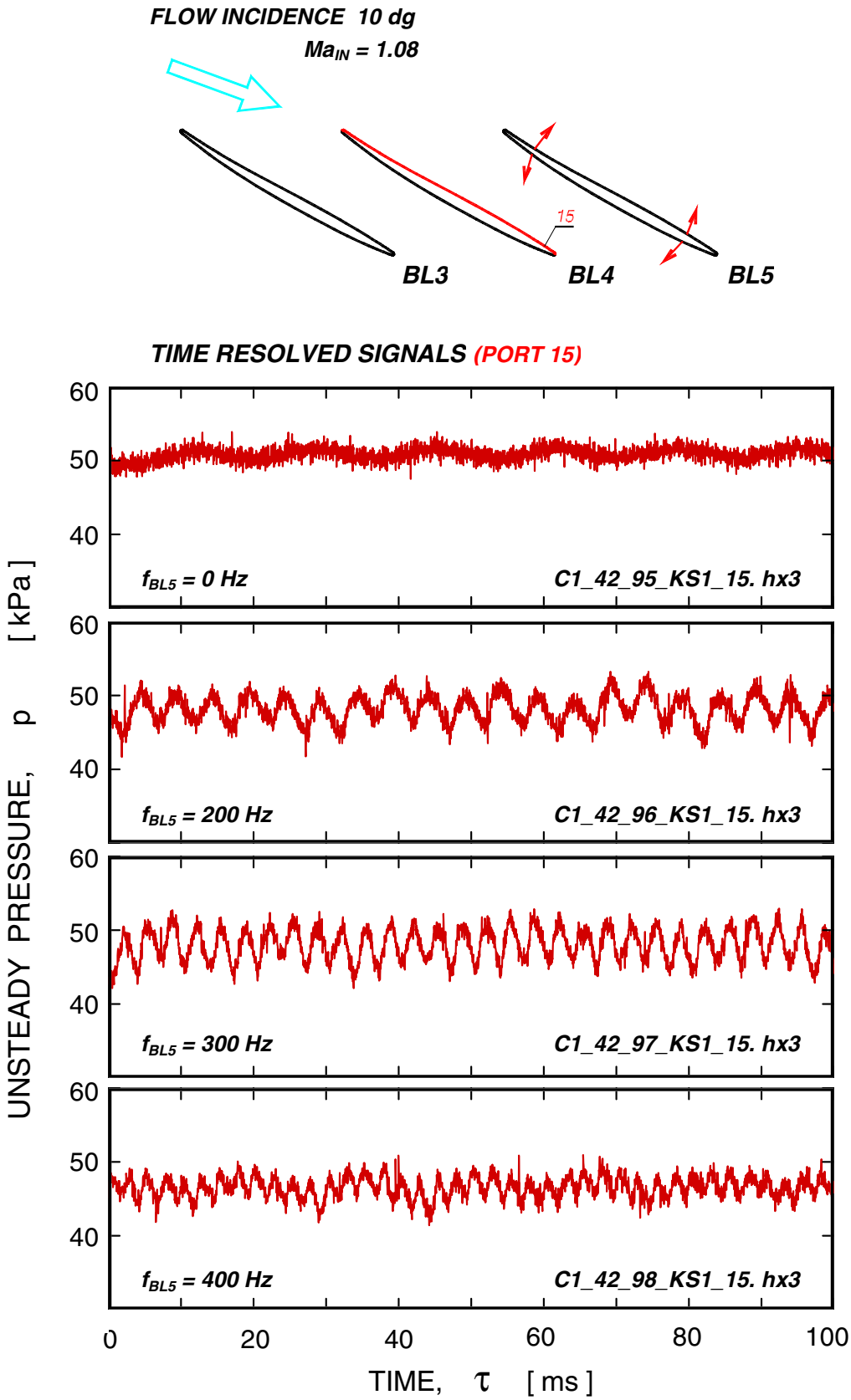

Fig. 7.2 Effects of blade oscillation frequency.

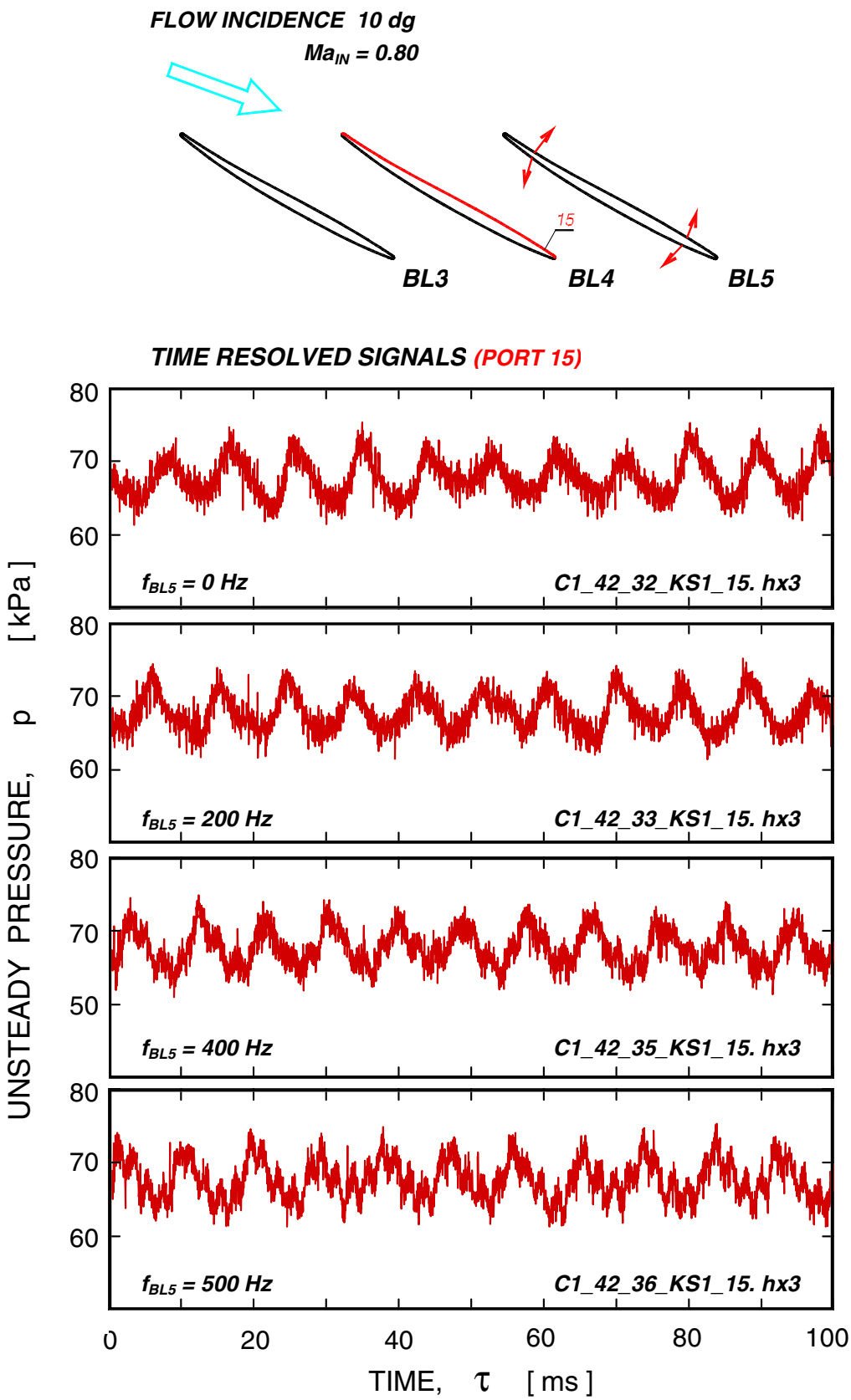

Fig. 7.3 Effects of blade oscillation frequency.

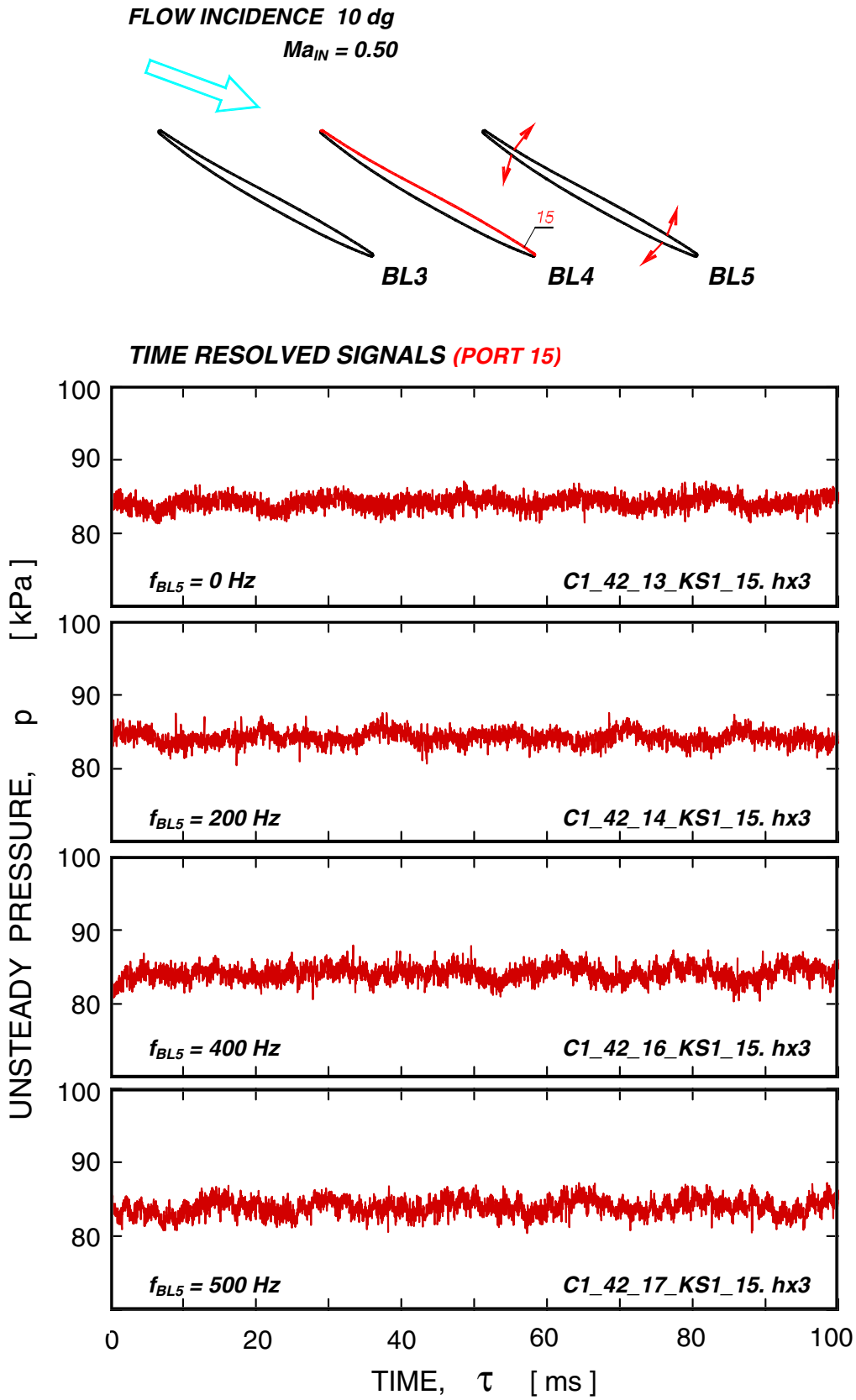

Fig. 7.4 Effects of blade oscillation frequency.

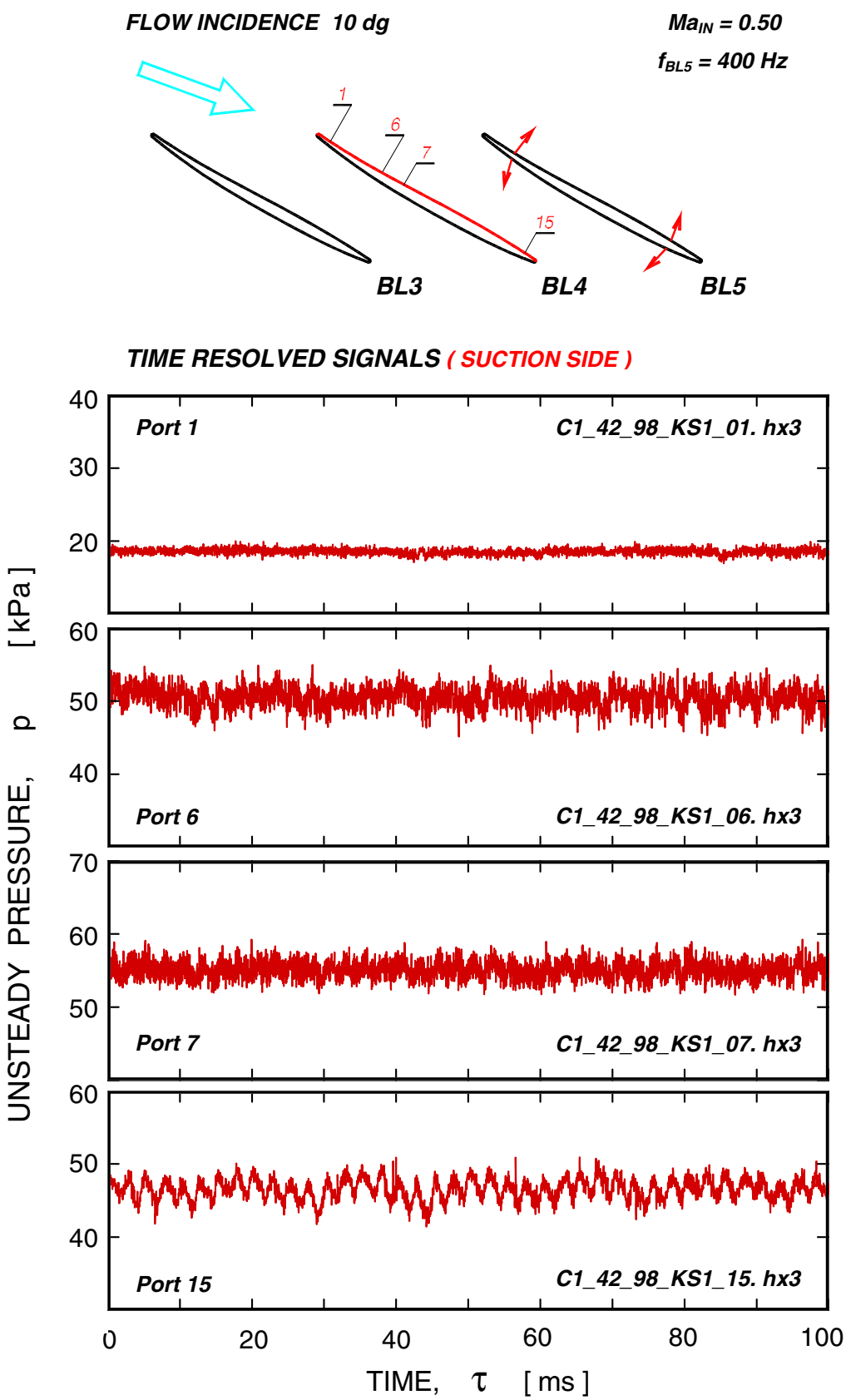

Fig. 7.5 Effect of position along blade chord.

VIEW FROM ABOVE

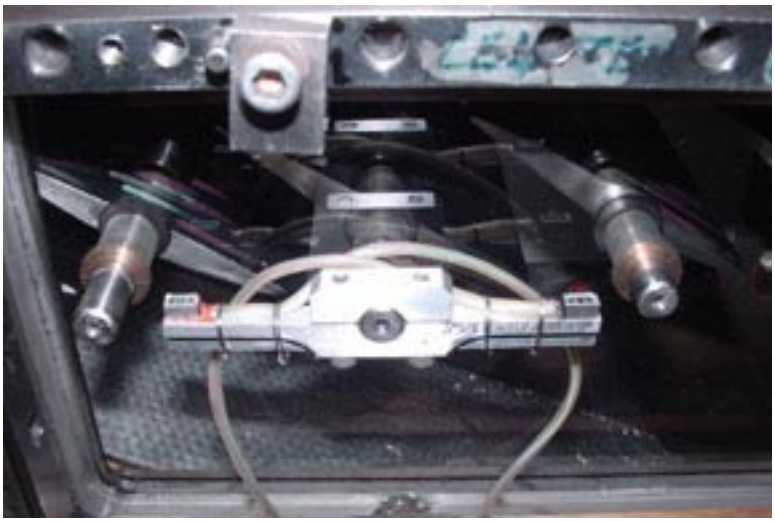

VIEW FROM BELOW

Fig. 7.6 Arm with accelerometers.

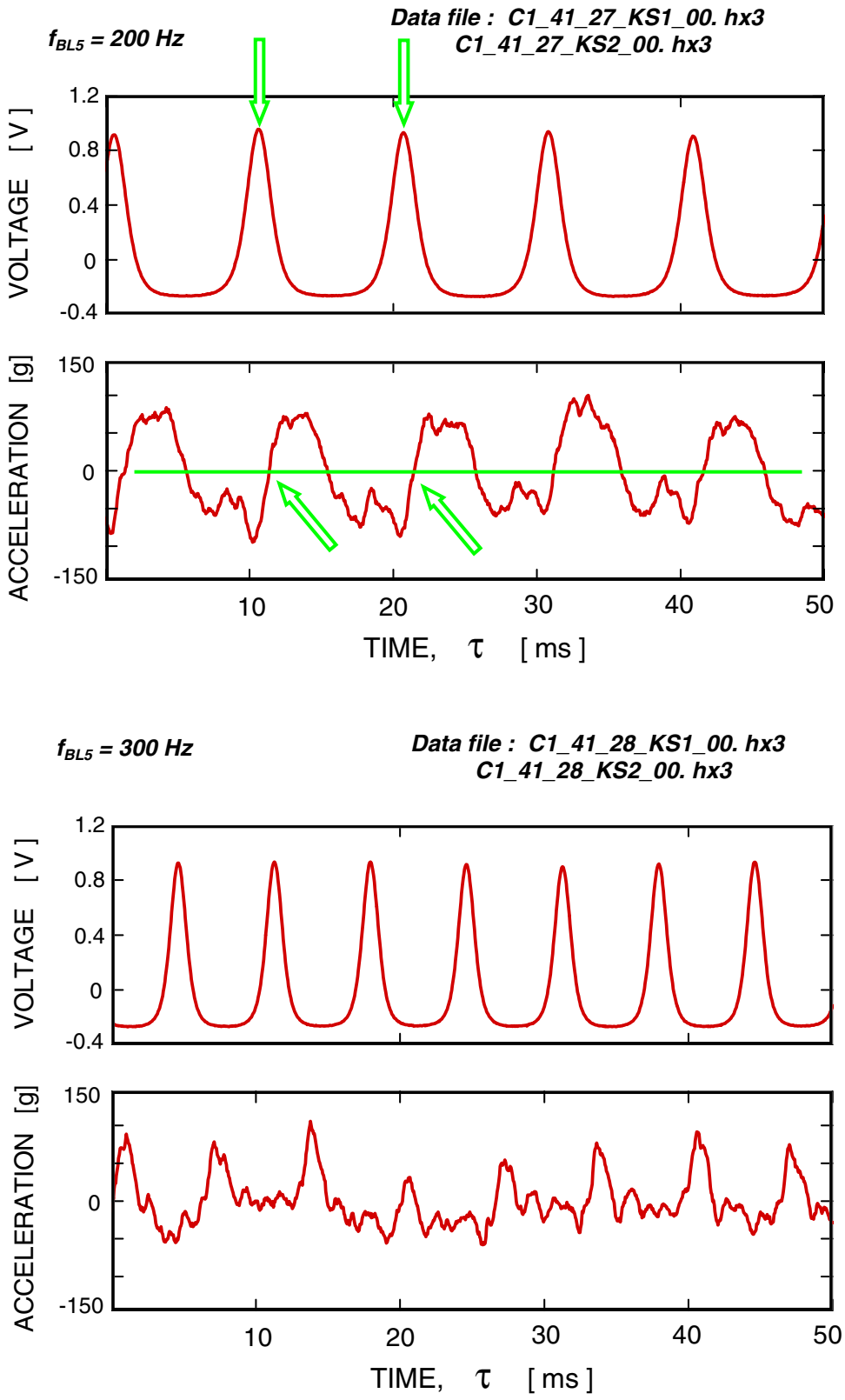

Fig. 7.7a Once-per-period and accelerometer signals.

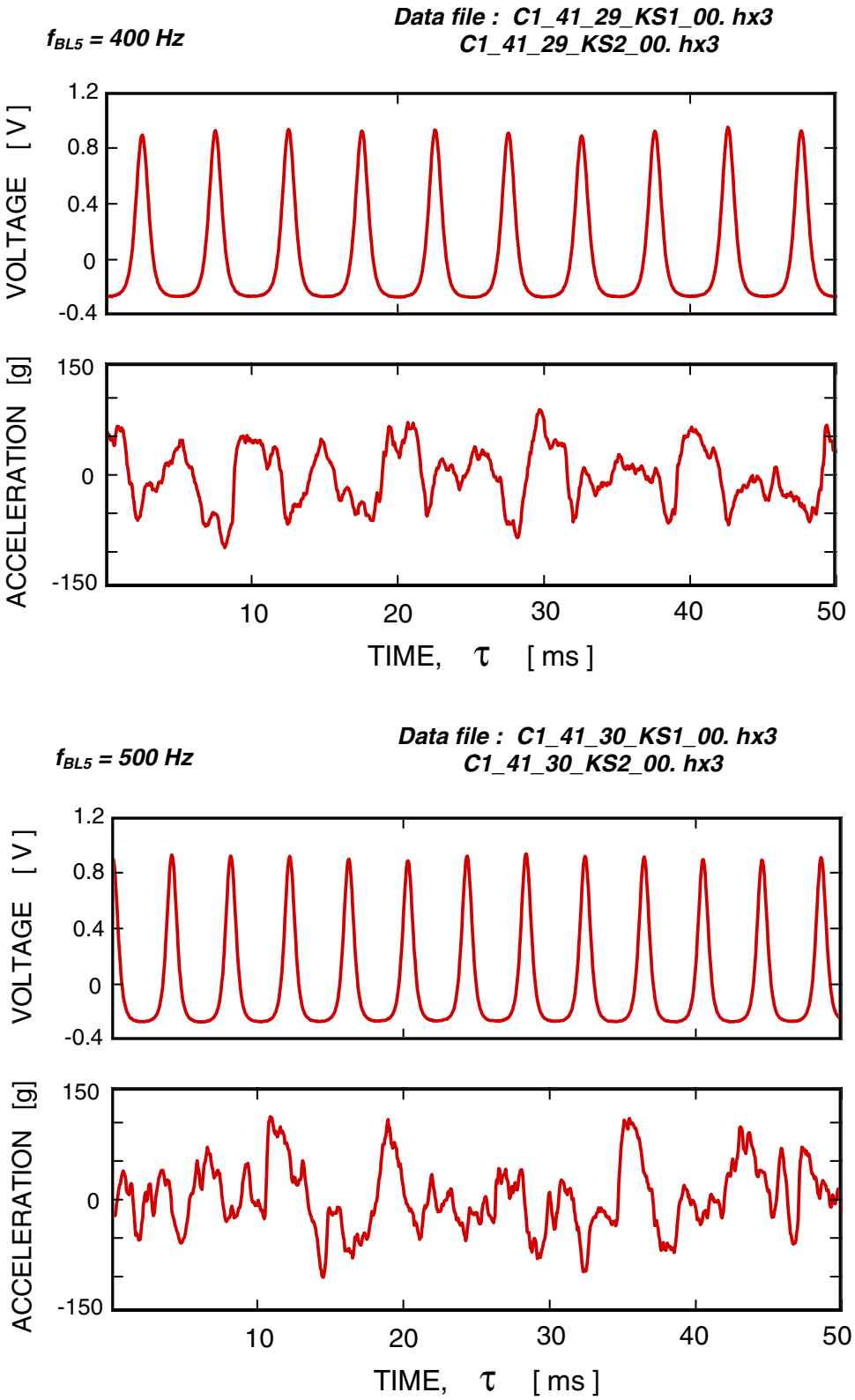

Fig. 7.7b Once-per-period and accelerometer signals.

Frequency	[Hz]	200	300	400	500
Amplitude	[mm]	0.42	0.42	0.42	0.42
Velocity	[m/s]	0.265	0.397	0.529	0.661
Acceleration	[m/s^2]	166.2	374.0	664.8	1038.8
Acceleration	[g]	16.9	38.1	67.8	105.9

Tab. 7.4 Expected acceleration parameters.

REPORT DOCUMENTATION PAGE

Form Approved
OMB No. 0704-0188

Public reporting burden for this collection of information is estimated to average 1 hour per response, including the time for reviewing instructions, searching existing data sources, gathering and maintaining the data needed, and completing and reviewing the collection of information. Send comments regarding this burden estimate or any other aspect of this collection of information, including suggestions for reducing this burden, to Washington Headquarters Services, Directorate for Information Operations and Reports, 1215 Jefferson Davis Highway, Suite 1204, Arlington, VA 22202-4302, and to the Office of Management and Budget, Paperwork Reduction Project (0704-0188), Washington, DC 20503.

1. AGENCY USE ONLY (*Leave blank*)

2. REPORT DATE
October 2002

3. REPORT TYPE AND DATES COVERED
Technical Memorandum

4. TITLE AND SUBTITLE
Methodology of Blade Unsteady Pressure Measurement in the NASA Transonic Flutter Cascade

5. FUNDING NUMBERS
WU–708–28–13–00

6. AUTHOR(S)
J. Lepicovsky, E.R. McFarland, V.R. Capece, T.A. Jett, and R.G. Senyitko

7. PERFORMING ORGANIZATION NAME(S) AND ADDRESS(ES)
National Aeronautics and Space Administration
John H. Glenn Research Center at Lewis Field
Cleveland, Ohio 44135–3191

8. PERFORMING ORGANIZATION REPORT NUMBER
E–13576

9. SPONSORING/MONITORING AGENCY NAME(S) AND ADDRESS(ES)
National Aeronautics and Space Administration
Washington, DC 20546–0001

10. SPONSORING/MONITORING AGENCY REPORT NUMBER
NASA TM—2002-211894

11. SUPPLEMENTARY NOTES
J. Lepicovsky and R.G. Senyitko, QSS Group, Inc., Cleveland, Ohio 44135; E.R. McFarland and T.A. Jett, NASA Glenn Research Center; and V.R. Capece, University of Kentucky, Department of Mechanical Engineering, Paducah, Kentucky 42002. Responsible person, J. Lepicovsky, organization code 5810, 216–433–1402.

12a. DISTRIBUTION/AVAILABILITY STATEMENT
Unclassified - Unlimited
Subject Categories: 07, 09 and 02 Distribution: Nonstandard
Available electronically at http://gltrs.grc.nasa.gov
This publication is available from the NASA Center for AeroSpace Information, 301–621–0390.

12b. DISTRIBUTION CODE

13. ABSTRACT ***(Maximum 200 words)***
In this report the methodology adopted to measure unsteady pressures on blade surfaces in the NASA Transonic Flutter Cascade under conditions of simulated blade flutter is described. The previous work done in this cascade reported that the oscillating cascade produced waves, which for some interblade phase angles reflected off the wind tunnel walls back into the cascade, interfered with the cascade unsteady aerodynamics, and contaminated the acquired data. To alleviate the problems with data contamination due to the back wall interference, a method of influence coefficients was selected for the future unsteady work in this cascade. In this approach only one blade in the cascade is oscillated at a time. The majority of the report is concerned with the experimental technique used and the experimental data generated in the facility. The report presents a list of all test conditions for the small amplitude of blade oscillations, and shows examples of some of the results achieved. The report does not discuss data analysis procedures like ensemble averaging, frequency analysis, and unsteady blade loading diagrams reconstructed using the influence coefficient method. Finally, the report presents the lessons learned from this phase of the experimental effort, and suggests the improvements and directions of the experimental work for tests to be carried out for large oscillation amplitudes.

14. SUBJECT TERMS
Transonic flutter cascade; Unsteady pressure measurement

15. NUMBER OF PAGES
55

16. PRICE CODE

17. SECURITY CLASSIFICATION OF REPORT
Unclassified

18. SECURITY CLASSIFICATION OF THIS PAGE
Unclassified

19. SECURITY CLASSIFICATION OF ABSTRACT
Unclassified

20. LIMITATION OF ABSTRACT